# Point and column aerosol radiative closure during ACE 1: Effects of particle shape and size

A. M. Fridlind[1] and M. Z. Jacobson

Department of Civil and Environmental Engineering, Stanford University, Stanford, California, USA

Received 30 November 2001; revised 1 August 2002; accepted 12 August 2002; published 4 February 2003.

[1] We used data collected during the First Aerosol Characterization Experiment (ACE 1) to study point and column aerosol radiative closure over the remote ocean. To test point closure, total and hemispheric backscattering coefficients calculated with a Mie single-scattering model were compared with measurements made by ship and aircraft at three wavelengths (400, 550, and 700 nm). On the ship, assuming spherical particles, calculated total scattering was usually within 10% of measurements (closure obtained in >80% of the cases) but calculated backscattering was usually 15–25% lower than measurements (closure obtained in <50% of the cases). When a model for particle nonsphericity was applied to the dried sea spray, assuming the particles to be ideal cubes or irregular convex and concave crystals resulted in overestimation of backscattering. However, when nonsphericity parameters were fit to the measurements, calculated backscattering was also usually within 10% of measurements (closure obtained in >80% of the cases). On the aircraft, however, calculated scattering and backscattering were usually lower than measurements by 20–45% regardless of assumed particle shape (closure obtained in <50% of the cases), likely owing to differences in the aerosol inlet penetration efficiencies to each instrument or unidentified uncertainties in the measured number size distributions or scattering coefficients. To test column closure, aerosol extinction profiles calculated from in situ observations (below 5.5 km) and satellite observations (above 5.5 km) were vertically integrated, and the resulting aerosol optical depth was compared with measurements made on the ship during two clear-sky days at three wavelengths (500, 778, and 862 nm). Calculated spectral optical depths were usually within 25% of measurements (closure obtained at one or more wavelengths on both days), and agreement at longer wavelengths was improved when satellite measurements were spectrally scaled using in situ model results. On both days, large sea salt particles produced a spectrally neutral aerosol optical depth in the marine boundary layer whereas smaller ammonium sulfate particles contributed to greater optical depth at shorter wavelengths in the overlying upper atmosphere. *INDEX TERMS:* 0305 Atmospheric Composition and Structure: Aerosols and particles (0345, 4801); 0360 Atmospheric Composition and Structure: Transmission and scattering of radiation; 3337 Meteorology and Atmospheric Dynamics: Numerical modeling and data assimilation; 3359 Meteorology and Atmospheric Dynamics: Radiative processes; *KEYWORDS:* aerosols, radiation, scattering coefficient, optical depth, backscattering coefficient, nonsphericity

**Citation:** Fridlind, A. M., and M. Z. Jacobson, Point and column aerosol radiative closure during ACE 1: Effects of particle shape and size, *J. Geophys. Res.*, *108*(D3), 4094, doi:10.1029/2001JD001553, 2003.

## 1. Introduction

[2] It is now well known that natural and anthropogenic aerosols significantly impact the earth's climate and photochemistry by directly scattering and absorbing solar radiation and by serving as cloud condensation nuclei, but much work remains to accurately quantify and predict these impacts [e.g., *Intergovernmental Panel on Climate Change*, 2001]. Because of the short temporal and spatial scales of aerosol heterogeneity, numerical models of aerosol optical behavior are required to make accurate quantifications of past and present global aerosol radiative effects, as well as predictions based on future emissions scenarios. An important goal of many field studies is thus to provide data that may be used to evaluate the ability of such models to represent the optical properties of ambient atmospheric aerosols. In the sense that agreement between model results and measurements "indicates that the model may be a suitable representation of the observed system," this may be referred to as a "closure study" [*Quinn et al.*, 1996a].

[1] Now at Earth Science Division, NASA Ames Research Center, Moffett Field, California, USA.


0148-0227/03/2001JD001553$09.00

Performing such studies on many regional aerosol types, both pristine and anthropogenically impacted, permits quantification of the uncertainties associated with calculating the integrated impact of aerosols on the past, present, and future global radiative budget.

[3] For the studies presented here, we applied a Mie single-scattering model to calculate point and column aerosol optical properties from first principles. A test of point closure using a Mie model generally requires concurrent field measurements of (1) number size distribution, (2) size-distributed chemical composition, (3) atmospheric temperature and relative humidity, and (4) optical properties. Data on size-resolved aerosol mixing state and morphology are also often required to fully constrain calculations but are usually unavailable. Field data sets that meet all or most of the four basic data requirements and have been used with a Mie model to test point closure include PSI 91 and MAGE 92 [*Quinn et al.*, 1995], RITS [*Quinn et al.*, 1996b], ACE 1 [*Quinn and Coffman*, 1998], SCAR-B [*Ross et al.*, 1998], TARFOX [*Hartley et al.*, 2000], SCOS [*Collins et al.*, 2000a], ACE 2 [*Collins et al.*, 2000b], and Aerosols99 [*Quinn et al.*, 2001]. A test of column closure using a Mie model, by extension, generally requires profile measurements of (1) number size distribution, (2) size-distributed chemical composition, (3) atmospheric temperature and relative humidity, as well as (4) total or layer aerosol optical depth. Field data sets that have been used with a Mie model to test column closure include ASTEX [*Clarke et al.*, 1996] and ACE 2 [*Russell and Heintzenberg*, 2000, and references therein].

[4] In this work, we used data collected over the remote ocean during leg 2 of ACE 1 [*Bates et al.*, 1998a]. The ACE 1 experiment was designed to provide data for point and column closure studies and during leg 2 the aerosols were relatively simple from a chemical and morphological standpoint, with negligible dust, smoke, or soot. Expanding upon an existing study of point closure on the *Discoverer* ship during ACE 1 [*Quinn and Coffman*, 1998], we first applied a Mie model to calculate total scattering and hemispheric backscattering coefficients from the number size distribution and chemical composition measurements made by both ship and aircraft. We evaluated point closure by comparing the calculated scattering coefficients with measured values at three wavelengths (400, 550, and 700 nm). We next calculated aerosol optical depth by integrating the extinction profiles that we obtained by applying the Mie model to number size distribution and chemical composition gathered below 5.5 km (the maximum aircraft elevation) and using satellite measurements above 5.5 km. We evaluated column closure by comparing the calculated aerosol optical depth with measurements made from the ship at three wavelengths (500, 778, and 862 nm).

## 2. Field Data

[5] All ship, aircraft, and satellite data that we used were gathered over the Southern Ocean (40°–55°S, 135°–160°E) between November 16 and December 11, 1995 (Julian days 320.000–345.000 UTC). The ACE 1 data were gathered on two platforms: (1) the National Oceanic and Atmospheric Administration (NOAA) R/V Discoverer ship, and (2) the National Center for Atmospheric Research (NCAR) C-130 aircraft. We evaluated point closure with data from the full duration of leg 2 on the ship, as well as the duration of the only two flights of the aircraft that were near the ship under clear skies (flights 22 and 24). We then evaluated column closure during those two flights.

### 2.1. ACE 1 Aerosol Data

[6] Aerosol chemistry, number size distribution, and light scattering coefficients were measured on both ship and aircraft. On both platforms, a heated aerosol inlet collected ambient air, heated it to a lower relative humidity, and then supplied each aerosol instrument, increasing the likelihood that all instruments were observing the same number size distribution at the same relative humidity [*Bates et al.*, 1998a]. On the ship, the heated inlet sampled air through a mast 18 m above sea level [*Quinn and Coffman*, 1998]. The mast size cut was unknown, but number size distribution measurements had a size cut of ≈5 and light scattering measurements had a size cut of ≈10 (see section 2.1.1). On the aircraft, the heated inlet sampled air isokinetically from the starboard side of the aircraft and decelerated it, with a size cut of ≈3 in ambient diameter [*Blomquist et al.*, 2001]. On both platforms, some instruments required that the air stream be further dried prior to making measurements. Since the chemical, morphological, and optical properties of hygroscopic aerosols are especially sensitive to relative humidity, this is an important aspect of each measurement. Throughout this work, we refer to the relative humidity in the air stream supplied by the heated inlet as the ''inlet relative humidity,'' which was always drier than the relative humidity in the tropospheric air encountered by the ship or aircraft, referred to as the ''ambient relative humidity.'' When the inlet air stream was further heated prior to measurements by a particular instrument, we refer to this as the ''instrumental relative humidity.'' The air stream relative humidity and temperature sampled by each aerosol instrument on the ship and aircraft are listed in Table 1, along with instrument size resolution and averaging time duration. Differences between the instruments used to measure number size distribution and chemical composition on the ship and aircraft platforms resulted in differences between the specific model calculations required to evaluate point closure on each platform (see section 3.1).

#### 2.1.1. Ship Platform

[7] Aerosol chemical composition was measured with a 7-stage Berner-type cascade impactor, as reported by *Quinn et al.* [1998] and *Quinn and Coffman* [1998]. Mean diameters on each stage were 0.15, 0.32, 0.49, 0.89, 1.7, 3.3, and 7.4 (aerodynamic diameter at the inlet relative humidity), resolving the aerosol sizes that scatter light most efficiently. Ion chromatography was used to determine total soluble $Cl^-$, $Br^-$, $NO_3^-$, $SO_4^{2-}$, $CH_3SO_3^-$, $Na^+$, $NH_4^+$, $K^+$, $Mg^{2+}$, and $Ca^{2+}$. A mass closure study using gravimetric mass measured on the ship concluded that these ions accounted for the aerosol mass within the mean experimental uncertainty of ±40% [*Quinn and Coffman*, 1998], indicating that organics and insoluble matter could make significant unknown contributions (see section 3.2.4). Of the 21 chemistry samples used in this study, only 4 samples were continentally influenced, as defined by 2-hour mean radon concentrations

**Table 1.** ACE 1 Aerosol Measurements

| Variable | Air Stream | RH, % | T, C | Size Bins | Size Range, μm | Duration |
|---|---|---|---|---|---|---|
| Ship platform | ambient | 54–99 | 0–15 | | | |
| Chemistry | inlet | 19–51 | 12–30 | 7 | 0.15–7.4[a] | 16–40 h |
| Size distribution | | | | | | |
| Short DMPS | instrumental | 10 | ... | 9 | 0.005–0.029[b] | 30 min |
| Long DMPS | instrumental | 10 | ... | 16 | 0.020–0.43[b] | 30 min |
| APS | inlet | ... | ... | 25 | 0.84–4.7[a] | 30 min |
| Light scattering | inlet | ... | ... | 1 | <10[c] | 30 min |
| Aircraft platform | ambient | 4–81 | −17–11 | | | |
| Chemistry | inlet | ... | ... | 1–2 | 0.5–5[a] | 20–80 min |
| Size distribution | instrumental | ... | 40 | 233 | 0.15–7.7[b] | 40 s |
| Light scattering | inlet | 3–30 | 26–29 | 1 | <3[d] | 15 s |

[a]Range of size bin midpoints in terms of reported aerodynamic diameter.
[b]Range of size bin midpoints in terms of reported geometric diameter.
[c]Size cut of the impactor preceding the ship's nephelometer in terms of aerodynamic diameter.
[d]Approximate size cut of the aircraft's heated aerosol inlet in terms of geometric diameter at the ambient RH and T.

exceeding 100 mBq $m^{-3}$ [*Whittlestone et al.*, 1998], and the remaining samples were representative of pure maritime air. We assumed the relative humidity and temperature reported for the impactor to be representative of all inlet air streams on the ship.

[8] Aerosol number size distributions were measured in two separate inlet air streams, as reported by *Quinn et al.* [1998], *Quinn and Coffman* [1998], and *Bates et al.* [1998b]. Smaller particles were measured in one air stream with two differential mobility particle sizer (DMPS) instruments connected to particle counters. Measurement with these instruments required further drying the inlet air to 10% relative humidity. Data were reported in 25 partially overlapping size bins with mean diameters of 0.005–0.43 (geometric diameter at the instrumental relative humidity). Particles in the first 9 size bins (0.005–0.029) were separated by negative charge with a Vienna short-column DMPS and measured with a TSI Model 3025 particle counter. Particles in the remaining 16 size bins (0.02–0.43) were separated by positive charge with a TSI long-column DMPS and measured with a TSI Model 3010 particle counter. All reported DMPS data were corrected for diffusional losses and size-dependent counting efficiencies. Larger particles were measured in a separate inlet air stream with an aerodynamic particle sizer (APS) that reported number concentrations in 25 size bins with mean diameters of 0.84–4.70 (aerodynamic diameter at the inlet relative humidity). APS data at diameters larger than 5 were discarded due to interferences from phantom counts [*Quinn and Coffman*, 1998] (see section 3.2.4).

[9] Aerosol total scattering and hemispheric backscattering coefficients at 450, 550, and 700 nm were measured with a TSI Model 3563 3-wavelength integrating nephelometer after passing the inlet air stream through an impactor with a 10- size cut, as reported by *Quinn et al.* [1998] and *Quinn and Coffman* [1998].

[10] Total aerosol optical depths at 500, 778, and 862 nm were measured with a handheld Sun photometer designed and calibrated by the NOAA Climate Monitoring and Diagnostics Laboratory, as reported to the ACE 1 public archive by P. K. Quinn.

#### 2.1.2. Aircraft Platform

[11] Aerosol chemical composition was measured with a single filter (bulk measurement) or with an impactor preceding the filter (2-stage measurement), as reported by *Huebert et al.* [1998]. The impactor was usually in place with a size cut of 1 (assumed to be geometric diameter at the inlet relative humidity), followed by a filter to collect the remaining particles. Ion chromatography was used to determine total soluble $Cl^-$, $NO_3^-$, $SO_4^{2-}$, $CH_3SO_3^-$, $Na^+$, and $NH_4^+$. Sample exposure periods were 20–80 minutes at a single elevation of flight. Mass closure was not performed for lack of parallel gravimetric mass measurements.

[12] Aerosol number size distributions were measured with a Particle Measurement Systems LAS-X optical particle counter (OPC) that was modified for 256 channels, as reported by *Clarke et al.* [1998]. The air stream was diluted one-to-one with dry air and then heated to 40°C prior to measurement with the OPC, reducing the inlet relative humidity to its initial value multiplied by an estimated factor of 0.2 (equal to 0.5 times ≈0.4, based on the estimated reduction in saturation vapor pressure during heating from the inlet temperature of ≈25°C to the instrumental temperature of 40°C). Reported particle sizes assumed that submicron particles were ammonium bisulfate and supermicron particles were sea salt. Data were reported in 233 size bins with mean diameters of 0.15–7.7 μm (geometric diameter at the instrumental relative humidity).

[13] Aerosol total scattering and hemispheric backscattering coefficients at 450, 550, and 700 nm were measured with a TSI Model 3563 3-wavelength integrating nephelometer, as reported by *Baumgardner and Clarke* [1998]. We assumed the relative humidity and temperature reported for the nephelometer to be representative of all inlet air streams on the aircraft.

### 2.2. ACE 1 Meteorological Data

[14] Profiles of pressure, temperature, and relative humidity were measured from the surface to ≈20 km using the NCAR Integrated Sounding System (ISS) high vertical resolution balloons, as reported to the ACE 1 public archive by the NCAR Atmospheric Technology Division. The data were reported at 50 m resolution with an important correction for low-level humidity sensor errors using independent surface data gathered on the ship.

[15] At the surface, atmospheric temperature and relative humidity were measured with the ship's RM Young sensors and barometric pressure was measured with a Qualimetrics

sensor, as reported to the ACE 1 public archive by J. E. Johnson and T. S. Bates.

### 2.3. SAGE II Satellite Data

[16] Sunset profiles of aerosol extinction coefficients in the upper free troposphere and stratosphere were reported at 385, 453, 525, and 1020 nm from observations of the SAGE II satellite (data version 5.96).

## 3. Point Closure

[17] We evaluated point closure using all data for which number size distribution, chemical composition, and scattering coefficient measurements were simultaneously available, including 887 points on the ship, 19 points on flight 22, and 51 points on flight 24. Since all measurements were made from the aerosol inlet on each platform, point closure was evaluated at the inlet relative humidity. Compared with the previous study of point closure on the ship [*Quinn and Coffman*, 1998], we expanded the number of aerosol species included from the 20 considered in that study to 44 (Table 2) and we expanded the number of modeled data points from the 22 considered in that study to 887. Owing to the uniformity of chemistry in the optically important particles in the MBL throughout leg 2 of the ACE 1 experiment, we modeled more data points by using the 30-min scattering coefficient averaging time rather than the multiple-hour chemical composition averaging time (see Table 1). Our sensitivity tests indicated that changes in chemical composition throughout leg 2 of the ship's cruise usually affected calculated scattering coefficients on the ship by <2.5%. We are aware of no previously published point or column closure studies using data gathered on the aircraft.

[18] In the following sections we describe the point model (section 3.1), results and uncertainties (section 3.2), and evaluation of closure (section 3.3).

### 3.1. Point Model Description

[19] We used a Mie single-scattering model [*Toon and Ackerman*, 1981] to calculate the total scattering coefficient ($\sigma_s$) at each wavelength ($\lambda$) as the sum over each number size bin ($i$) of the product of the number of particles of a given diameter ($n(D_i)$), their cross-sectional area, and their Mie total scattering efficiency ($Q_s$),

$$\sigma_s(\lambda) = \sum_{i=0}^{N_D} n(D_i)\frac{\pi D_i^2}{4} Q_s\left(D_i, m_{j_i}, \lambda\right). \quad (1)$$

The Mie total scattering efficiency was in turn calculated from an integral of the intensity function for unpolarized light scattered by a homogeneous sphere ($|S_{11}(\theta, D_i, m_{j_i},\lambda)|^2$) over all angles ($\theta$) into which the light is scattered [e.g., *Bohren and Huffman*, 1983],

$$Q_s = \left(\frac{\lambda}{\pi D_i}\right)^2 \int_0^{\pi} \left|S_{11}\left(\theta, D_i, m_{j_i}, \lambda\right)\right|^2 \sin\theta d\theta. \quad (2)$$

The hemispheric backscattering coefficient ($\sigma_b$) was similarly calculated by limiting the integral over $\theta$ to the rear hemisphere ($\pi/2$ to $\pi$). The Mie total scattering and backscattering efficiencies were thus a unique function of particle diameter, wavelength, and the refractive index ($m_{j_i}$) in the chemistry size bin ($j$) corresponding to the number size bin ($i$).

**Table 2.** Aerosol Species in EQUISOLV II

| Aqueous | Ionic | Solid |
|---|---|---|
| $H_2O_{(aq)}$ | $H^+$ | $NH_4NO_{3(s)}$ |
| $H_2CO_{3(aq)}$ | $OH^-$ | $NH_4Cl_{(s)}$ |
| $H_2SO_{4(aq)}$ | $HCO_3^-$ | $NH_4HSO_{4(s)}$ |
| | $CO_3^{2-}$ | $(NH_4)_2SO_{4(s)}$ |
| | $NH_4^+$ | $(NH_4)_3H(SO_4)_{2(s)}$ |
| | $NO_3^-$ | $NH_4HCO_{3(s)}$ |
| | $HSO_4^-$ | $NaNO_{3(s)}$ |
| | $SO_4^{2-}$ | $NaCl_{(s)}$ |
| | $CH_3SO_3^-$ | $NaHSO_{4(s)}$ |
| | $Na^+$ | $Na_2SO_{4(s)}$ |
| | $Cl^-$ | $NaHCO_{3(s)}$ |
| | $Mg^{2+}$ | $Na_2CO_{3(s)}$ |
| | $Ca^{2+}$ | $MgCl_{2(s)}$ |
| | $K^+$ | $Mg(NO_3)_{2(s)}$ |
| | $Br^-$ | $MgSO_{4(s)}$ |
| | | $MgCO_{3(s)}$ |
| | | $Ca(NO_3)_{2(s)}$ |
| | | $CaCl_{2(s)}$ |
| | | $CaSO_{4(s)}$ |
| | | $CaSO_4-2H_2O_{(s)}$ |
| | | $CaCO_{3(s)}$ |
| | | $KNO_{3(s)}$ |
| | | $KCl_{(s)}$ |
| | | $KHSO_{4(s)}$ |
| | | $K_2SO_{4(s)}$ |
| | | $KHCO_{3(s)}$ |
| | | $K_2CO_{3(s)}$ |

[20] To evaluate equation (1), the light scattering averaging time was used on each platform. A "point" was thus defined as the air mass observed over 30 min on the ship and 15 s on the aircraft. The measured number size distribution resolution was also used on each platform (see Table 1): $N_D$ = 49 on the ship, less than the sum of total size bins due to overlapping size ranges, and $N_D$ = 233 on the aircraft. On the ship, the 30-min scattering averaging periods directly matched the number size distribution averaging periods. On the aircraft, the 15-s scattering averaging periods were matched to a temporally overlapping 40-s number size distribution. Due to the extended time between number size distribution measurements made at 40°C on the aircraft (elapsed during sequential measurements at 150°C and 300°C), a light scattering observation never overlapped more than one number size distribution observation. Chemistry data were assigned on the ship using the temporally nearest observation. Thus for the short periods between adjacent chemistry samples, the temporally nearest chemistry sample was considered adequate. On the aircraft, however, due to larger changes in chemistry vertically, only measurements made during a chemistry sampling period were used.

[21] We used the EQUISOLV II thermodynamic equilibrium model [*Jacobson*, 1999a, 1999b] to calculate aerosol refractive index ($m_j$) in equation (2) at the appropriate temperature and relative humidity, as well as aerosol density ($\rho_j$) and volume ($V_j$) in each chemistry size bin ($j$). To calculate aerosol properties from the measured ionic composition in each chemistry size bin, EQUISOLV II employs the Zdanovskii-Stokes-Robinson equation to estimate liquid water content, Bromley's method to estimate mean mixed

activity coefficients, and the partial molar refraction method to estimate the real refractive index of mixed solutions. The model inputs were temperature, relative humidity, and the ionic mass of $Na^+$, $Cl^-$, $Ca^{2+}$, $Mg^{2+}$, $K^+$, $Br^-$, $SO_4^{2-}$, $CH_3SO_3^-$, $NH_4^+$, and $NO_3^-$ in each of the available size bins. Charge imbalances in each size bin were attributed to unmeasured $H^+$ and $CO_3^{2-}$. Possible aerosol species included aqueous-, ionic-, and solid-phase species (see Table 2). Solids were assumed to form only when the relative humidity fell below their crystallization relative humidity (CRH).

[22] Particles on a given impactor stage were always assumed to be a well-mixed internal mixture of the measured species. This appeared to be a good assumption for the particles in the free troposphere (FT), which were composed primarily of ammonium sulfates, and also for supermicron particles in the marine boundary layer (MBL), which were composed primarily of sea salt. However, it may have been less accurate for submicron particles in the MBL, where external mixtures of ammonium sulfate and sea salt were observed to exist during ACE 1 [*Berg et al.*, 1998]. However, assumed mixing state had minor influence on the results presented here since optical properties were dominated by sea spray in the MBL, as previously reported by *Murphy et al.* [1998] and *Quinn et al.* [1998]. Our sensitivity tests indicated that all secondary species put together usually affected calculated scattering coefficients by <3% throughout leg 2 of the ship's cruise.

[23] When number size distributions and impactor size cuts were reported in terms of aerodynamic size (Table 1), we estimated the geometric diameter ($D_i$) from the reported aerodynamic diameter ($D_{i,a}$) and the density calculated in the corresponding chemistry size bin ($\rho_{j_i}$),

$$D_i = \frac{D_{i,a}}{\sqrt{\rho_{j_i}}}. \tag{3}$$

Similarly, when number size distributions were reported at the instrumental relative humidity, we estimated the diameter at the inlet relative humidity ($D_i$) from the reported diameter at the instrumental relative humidity ($D_{i,d}$) and the volume change calculated in the corresponding chemistry size bin between the respective instrumental and inlet relative humidities ($V_{j_i,d}$ and $V_{j_i}$),

$$D_i = D_{i,d}\left(\frac{V_{j_i}}{V_{j_i,d}}\right)^{1/3}. \tag{4}$$

We calculated the volume in each chemistry size bin from density data contained in EQUISOLV II for the water and aerosol species predicted by the model at the respective relative humidities.

### 3.2. Point Model Results

[24] In this section we describe three important adjustments made to the measurements and the model prior to evaluation of point closure. First, based on our previous study of aerosol chemistry during ACE 1, we adjusted the ionic composition measurements to account for the significant effect of experimental uncertainties on calculated aerosol properties (section 3.2.1). Second, we adjusted the model to account for the documented nonideal response of the integrating nephelometer instruments (section 3.2.2). And third, we fit a model parameterization to account for likely sea spray nonsphericity at the dry inlet relative humidity (section 3.2.3). The incremental effect of these adjustments is shown in Figures 1 and 2. Model results with the standard assumption of spherical particles (no fit model parameters) are also shown in time series for the 25-day cruise of the ship in Figure 3 and for both flights of the aircraft in Figure 4, along with the relative humidity at which measurements were made and the elevation of the

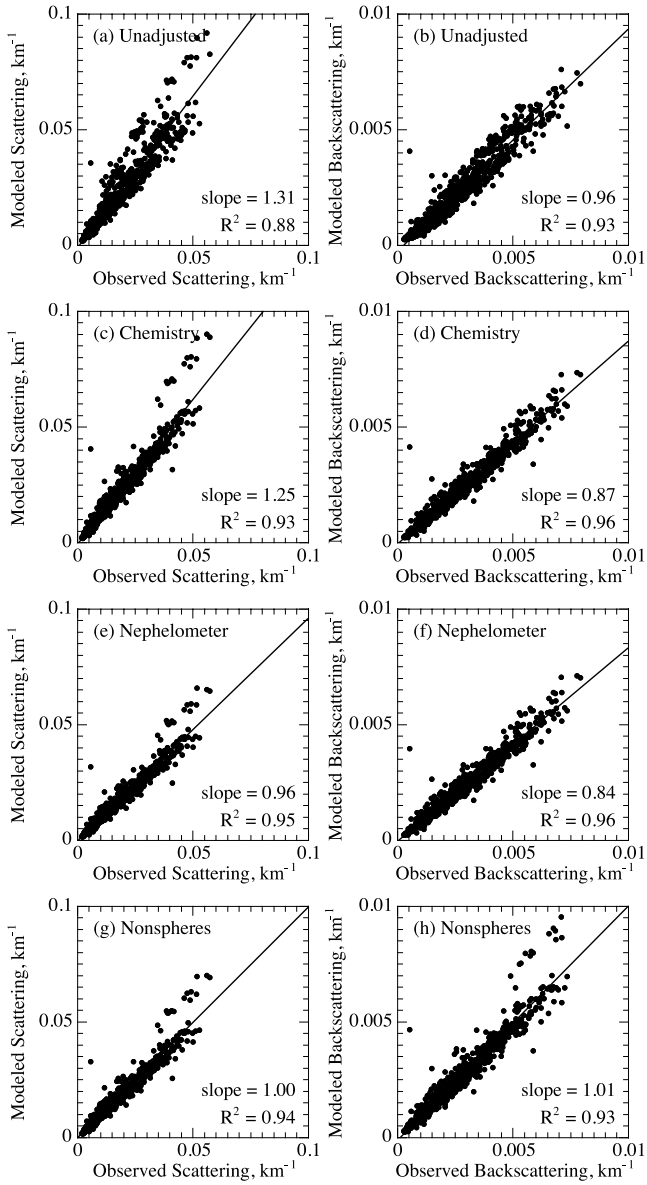


**Figure 1.** Calculated versus measured 550-nm total scattering and hemispheric backscattering coefficients at the inlet relative humidity on the ship: calculated values with no adjustments (a and b), with charge-balanced chemistry (c and d), accounting for nephelometer nonidealities (e and f), and assuming nonspherical particle parameters fit to data (g and h).

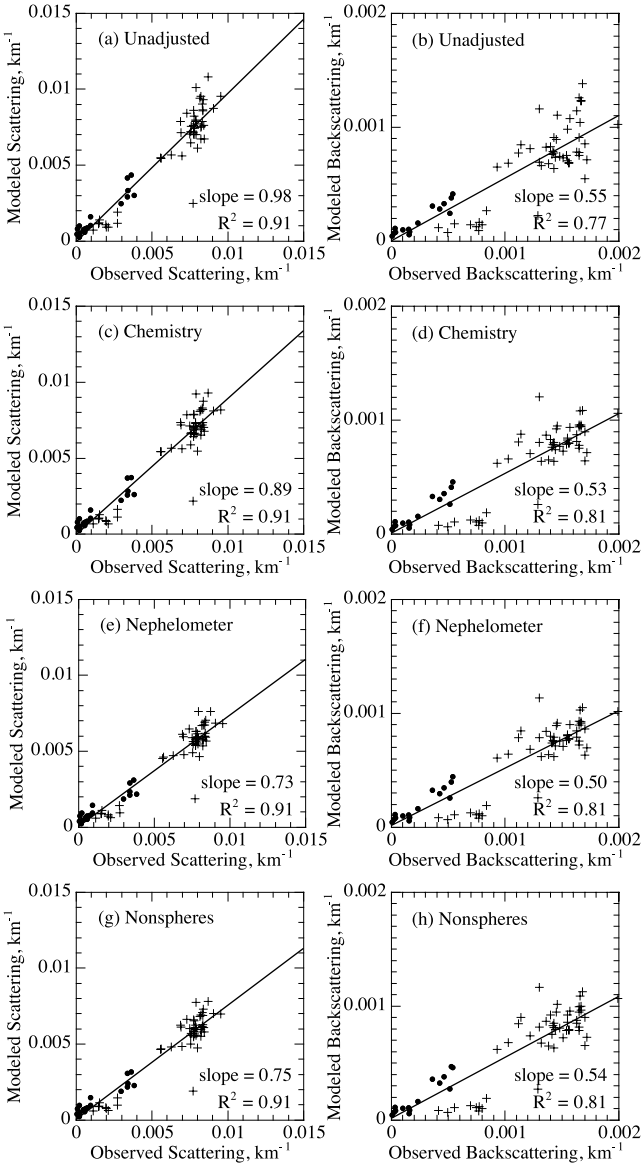


**Figure 2.** Calculated versus measured 550-nm total scattering and hemispheric backscattering coefficients at the inlet relative humidity on the aircraft during flight 22 (circles) and flight 24 (crosses): calculated values with no adjustments (a and b), with charge-balanced chemistry (c and d), accounting for nephelometer nonidealities (e and f), and assuming nonspherical particle parameters fit to the ship data (g and h).

aircraft. At the end of this section we summarize the sensitivity of the point model results to experimental uncertainties in input data and chemical composition assumptions (section 3.2.4).

### 3.2.1. Chemistry Adjustment

[25] On both ship and aircraft, we first initialized the chemistry samples with the measured ionic concentrations (Figures 1a, 1b, 2a, and 2b). However, our previous modeling study of aerosol composition on the ship during ACE 1 [*Fridlind and Jacobson*, 2000] demonstrated that charge imbalances induced by experimental uncertainty in the major sea salt ions often resulted in significant discontinuities in modeled pH from one size bin to the next. Thus, we subsequently initialized the aerosol phase using a charge-balancing procedure similar to the one described in that work: (1) $Cl^-$, $Mg^{2+}$, $Ca^{2+}$, $K^+$, and sea salt $SO_4^{2-}$ were scaled to measured $Na^+$ using standard sea salt composition [*Stumm and Morgan*, 1996]; (2) $Br^-$ was not permitted to exceed the sea salt $Br^-$:$Na^+$ ratio, but was not raised if it was depleted [e.g., *Ayers et al.*, 1999]; (3) all secondary species, including non-sea-salt $SO_4^{2-}$ (defined as that exceeding the sea salt ratio to $Na^+$), $CH_3SO_3^-$, $NH_4^+$, and $NO_3^-$, were unchanged; (4) any remaining imbalances were attributed to unmeasured $H^+$ and $CO_3^{2-}$; and (5) $HCl_{(g)}$ was permitted to escape or be absorbed until thermodynamic equilibrium was achieved.

[26] Initializing with this procedure increased the $R^2$ correlation coefficient between calculated and measured aerosol optical properties at the inlet relative humidity on the ship (Figures 1c and 1d versus Figures 1a and 1b) but was less important on the aircraft (Figures 2c and 2d versus Figures 2a and 2b). In the free troposphere, where many of the aircraft samples were gathered, negligible sea salt was present, so the procedure had no effect. Due to its importance to model results in the MBL and our belief that the physical properties of the aerosols were better represented, this procedure was adopted for all further evaluation of point and column closure. The sensitivity of results to the procedure is discussed further below (see sections 3.2.4 and 3.3).

### 3.2.2. Nephelometer Nonidealities

[27] We hypothesized that the model's consistent overestimation of measured total scattering on the ship (Figure 1c) was due to documented nephelometer nonidealities [*Anderson et al.*, 1996; *Heintzenberg and Charlson*, 1996; *Anderson and Ogren*, 1998], which were shown by *Quinn and Coffman* [1998] to be important to point closure on the ship during ACE 1. While nephelometer angular nonidealities have relatively little effect on hemispheric backscattering measurements, they may cause total scattering measurements to underestimate actual values by up to 40% for 10 μm particles since they scatter primarily in the forward direction where the instrument does not sense the scattered light. The angular sensitivity functions shown in Figure 4b of *Anderson et al.* [1996] ($f_s(\theta)$ and $f_b(\theta)$) were thus used to recalculate the total scattering and backscattering efficiencies. In equation (2), for instance, $\sin\theta$ was thus replaced with $f_s(\theta)$.

[28] When angular nonidealities were accounted for, calculated total scattering coefficients decreased by about 30% on the ship (Figure 1e versus Figure 1c) and 15% on the aircraft (Figure 2e versus Figure 2c) while calculated backscattering coefficients were reduced by less than 5% on both platforms (Figure 1f versus Figure 1d and Figure 2f versus Figure 2d). The angular nonidealities affected measurements on the ship more than on the aircraft owing to the larger particles sampled by the ship. Fewer large particles were sampled by the aircraft since they were not present in the FT and did not penetrate the aerosol inlet efficiently in the MBL.

[29] Whereas agreement between calculated and measured total scattering coefficients was improved by accounting for angular nonidealities on the ship, as hypothesized, it

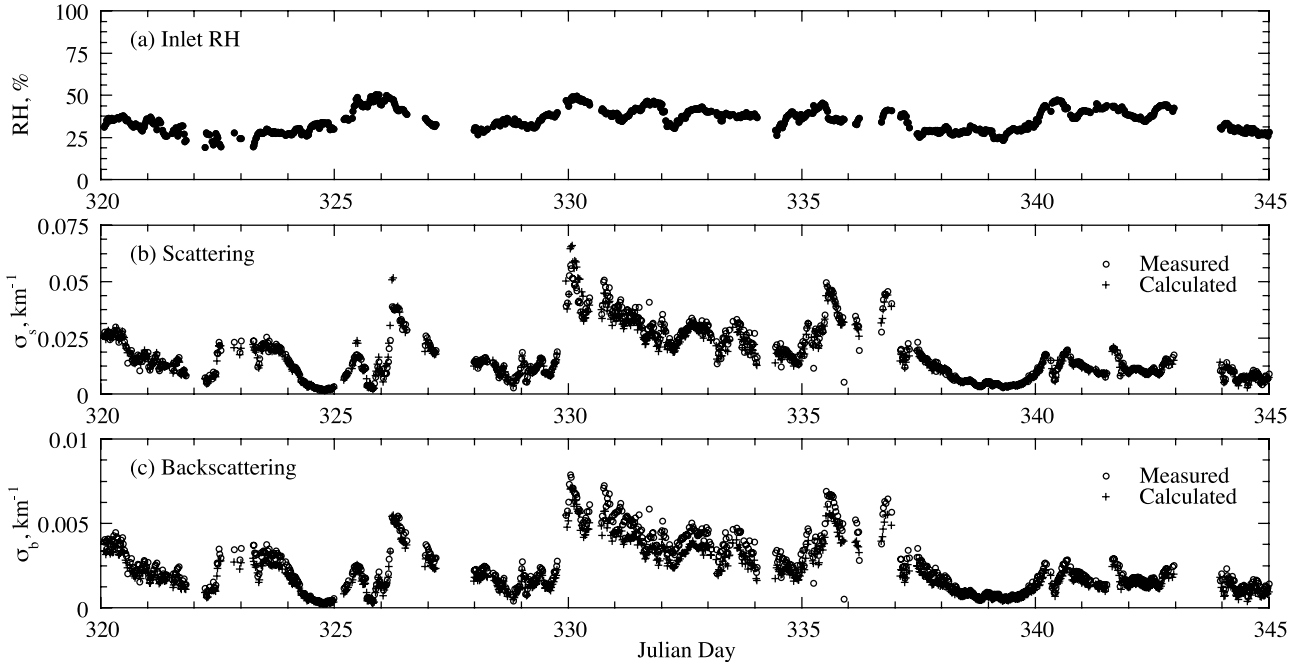


**Figure 3.** The inlet relative humidity on the ship, and the calculated and measured 550-nm total scattering and hemispheric backscattering coefficients. Calculated values account for chemistry adjustments and nephelometer nonidealities (same results shown in Figures 1e and 1f).

was worsened on the aircraft. However, we consider the worsened agreement on the aircraft to be indicative of other uncertainties, as discussed below (see section 3.3).

### 3.2.3. Particle Nonsphericity

[30] We next hypothesized that the model's persistent underprediction of backscattering on the ship (Figure 1f) was due to the effect of particle nonsphericity at the inlet relative humidity (see Figure 3), which was usually below the ≈45% CRH of sea salt [*Tang et al.*, 1997]. In general, deviations from particle sphericity affect backscattering more than total scattering and even small deviations from sphericity may increase hemispheric backscattering [e.g., *Bohren and Singham*, 1991; *Pilinis and Li*, 1998]. To account for the possible effect of nonsphericity on the calculated scattering coefficients, we applied the parameterization that *Pollack and Cuzzi* [1980] developed for polydisperse populations of randomly oriented nonspherical particles.

[31] To apply the parameterization, the number size distribution of nonspherical particles must first be expressed in terms of volume-equivalent sphere diameter ($D_{i,s}$). Assuming nonspherical particles on the ship, geometric diameters reported for the DMPS instruments were adjusted to the diameters of volume-equivalent spheres to first order by dividing by a dynamic shape factor $\chi$ [*Kelly and McMurry*, 1992],

$$D_{i,s} = \frac{D_i}{\chi}. \tag{5}$$

Similarly, aerodynamic diameters reported for the APS instrument were adjusted to the aerodynamic diameters of volume-equivalent spheres ($D_{i,a,s}$) to first order by multiplying by the square root of a dynamic shape factor [*Cheng et al.*, 1990],

$$D_{i,a,s} = D_{i,a}\sqrt{\chi}. \tag{6}$$

Dynamic shape factors were chosen based on assumed particle shape [*Hinds*, 1982; *Marshall et al.*, 1991]. No correction was made to diameters reported for the OPC instrument on the aircraft.

[32] The parameterization is then controlled by three values: (1) $x_o$, which is the value of particle circumference over wavelength below which nonsphericity is accounted for simply by applying Mie theory to volume-equivalent spheres and above which more complex calculations are made; (2) $r$, which approximates the ratio of the surface area of the nonspherical particle to that of its volume-equivalent sphere; and (3) $G$, which approximates the ratio of light transmitted into the forward hemisphere to that transmitted into the rear hemisphere. *Pollack and Cuzzi* [1980] fit these three values to the experimental scattering phase functions that have been reported for a limited number of particle shapes, including cubes, irregular convex and concave crystals, and flakes.

[33] When we assumed the particles to be cubes ($x_o = 4$, $r = 1.3$, $G = 2$, and $\chi = 1.08$), the calculated scattering phase function for a typical ACE 1 size distribution closely matched experimental results for similarly sized cubes (compare Figure 5 with that of *Pollack and Cuzzi* [1980]), but backscattering was overpredicted by more than a factor of two. Taking this to indicate that the aerosols during ACE 1 were not ideal cubes, we then assumed the shape to be more spherical. Assuming the particles to resemble the irregular convex and concave crystals studied by *Pollack*

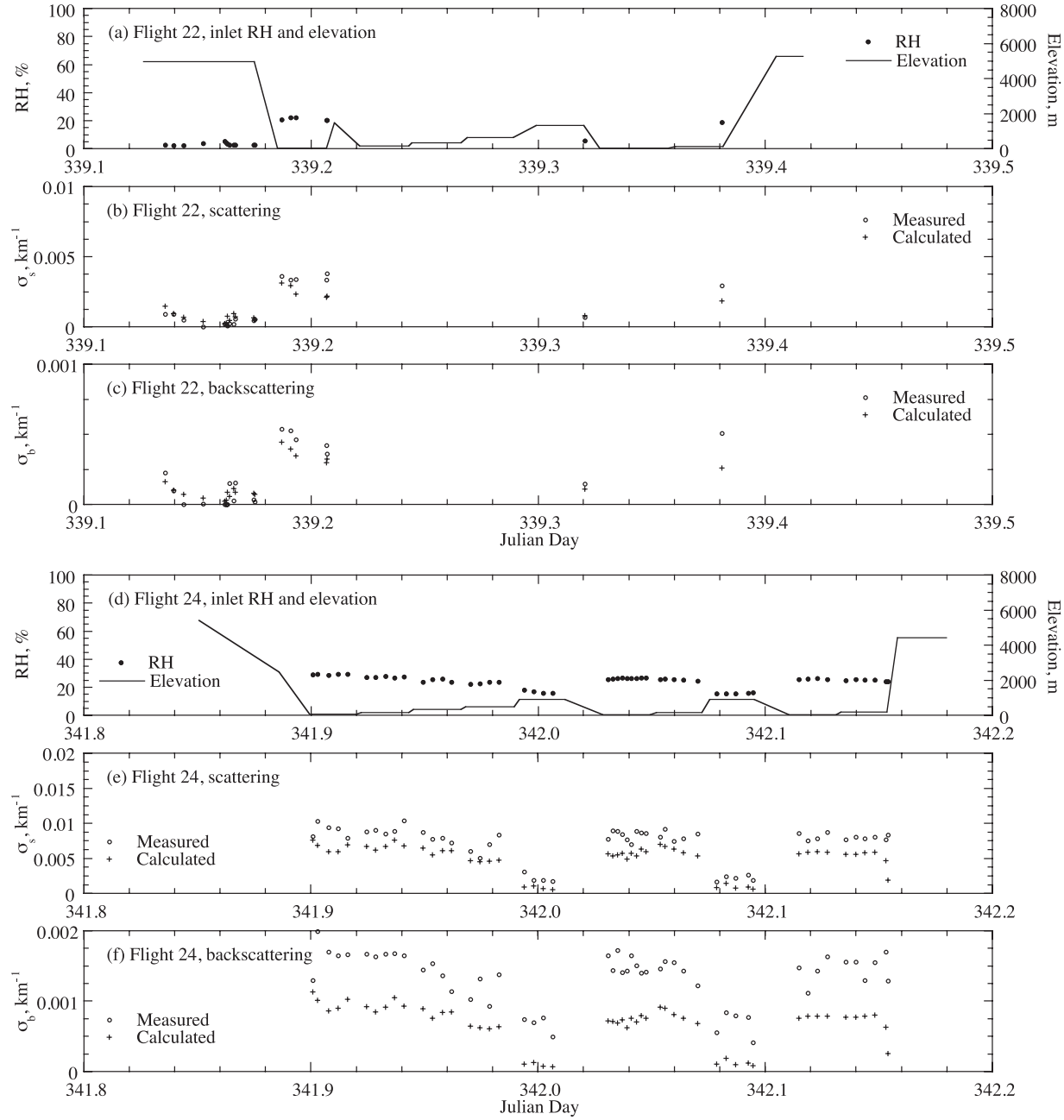


**Figure 4.** The inlet relative humidity and elevation of the aircraft, and the calculated and measured 550-nm total scattering and hemispheric backscattering coefficients during flight 22 (a–c) and flight 24 (d–f). Calculated values account for chemistry adjustments and nephelometer nonidealities (same results shown in Figures 2e and 2f).

*and Cuzzi* [1980] ($x_o$ = 10, $r$ = 1.3, $G$ = 4, and $\chi$ = 1.065) reduced overprediction of backscattering to ≈22%. No other previously studied shapes better reproduced measured backscattering, but a best fit of the parameter values to match measurements on the ship ($x_o$ = 11, $r$ = 1.1, $G$ = 5, and $\chi$ = 1.015) was able to simultaneously account for both backscattering and total scattering (Figures 1g and 1h). The corresponding phase function is nearer that of spheres than cubes (Figure 5), but cannot be considered uniquely determined based on the limited phase function information that we used here to estimate the parameters. Whereas *Pollack and Cuzzi* [1980] report that fitting their three parameters to the full experimental phase function gave unique values for each particle shape they studied, we would not assume that to be the case when the parameters are fit using only the integrated total scattering and hemispheric backscattering as we have done here for lack of more information.

[34] We would also not necessarily expect the best-fit parameters from the ship data gathered in the MBL to be as appropriate in the FT, where the chemical composition of the particles was primarily ammonium sulfate, likely with a different characteristic shape if solid [e.g., *Perry et al.*, 1978]. However, most aircraft samples were gathered in the MBL (Figure 4) and nonsphericity had little influence on

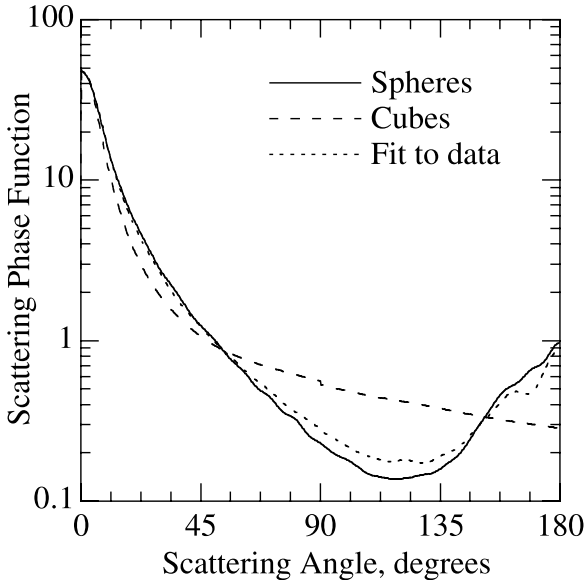


**Figure 5.** The phase functions calculated for a typical ACE 1 aerosol sample on the ship assuming that the aerosols were spheres (solid line) versus applying the *Pollack and Cuzzi* [1980] parameterization to model the phase function for cubic particles (dashed line) and nonspherical particles fit to data (dotted line, see section 3.2.3).

results in the FT due to the small size of the particles. Averaged over both FT and MBL, when the best-fit parameters from the ship data were used, calculated backscattering was increased by only ≈4% (Figure 2h versus Figure 2f).

[35] While we have shown that it is possible to fit a parameterization for nonsphericity to bring the model calculations in line with measured backscattering on the ship, as hypothesized, we are unable to prove that nonsphericity was in fact responsible for enhanced backscattering. Previous point closure studies have also found that assuming sphericity under dry aerosol sampling conditions resulted in underestimation of backscattering in marine environments [*Quinn et al.*, 1995; *Quinn and Coffman*, 1998], and it seems likely that at least some solids were present at the low inlet relative humidity during ACE 1. However, no current laboratory studies allow us to better evaluate our model representation of the effect of nonsphericity on the optical properties of dried sea spray during ACE 1. Studies of pure $NaCl_{(s)}$ aerosols dried in the laboratory indicate that they may be rounded cubes [*Tang et al.*, 1977], that they may contain pockets of liquid water [*Weis and Ewing*, 1999], and that their optical behavior may differ from that of spheres [*Perry et al.*, 1978]. However, dried aerosols generated from real sea water in the laboratory appear to behave differently from pure $NaCl_{(s)}$ [*Quinby-Hunt et al.*, 1997], and ambient marine aerosols may further differ from laboratory aerosols generated from real or artificial seawater due to greater quantities of primary and secondary organic and inorganic matter. Micrographs of sea spray aerosols dried in the field suggest all manner of possible shapes [e.g., *McInnes et al.*, 1994; *Pósfai et al.*, 1994; *von Hoyningen-Huene and Posse*, 1997; *Ebert et al.*, 2000] but seem highly prone to post-sampling processes and in any case cannot substitute for experimentally determined scattering phase function data, which are currently unavailable.

#### 3.2.4. Point Sensitivity Tests

[36] *Quinn and Coffman*'s [1998] previous study of point closure on the ship provided a tabulation of experimental uncertainties associated with aerosol measurements and other model inputs, including measurement of the particle size distributions and inlet temperature and relative humidity. We performed a similar analysis on both ship and aircraft (Table 3), but with at least two important differences. First, whereas they consider submicron and supermicron aerosol separately, we have not done so. This would have required extensive additional modeling to account for the size cut and inlet efficiencies of the impactor used to separate the particles since there is no 1-micron minimum in the scattering and backscattering size distributions (Figure 6). Second, we conservatively considered our charge-balanced aerosol composition (see section 3.2.1) to be "true," with no associated uncertainty. The comparison to results with the unadjusted chemistry and also possible organic content is included separately in Table 3 to establish the sensitivity of model results to this assumption.

[37] As a simple first-order estimate of the possible effect of organics on model results, we assumed that 10% and 40% of the dry mass of all aerosols was organic matter. Direct observations of organic matter in particles >0.5 μm in clean marine air have indicated about 10% organic content on a dry mass basis [*Middlebrook et al.*, 1998; *Oppo et al.*, 1999; *Neusüß et al.*, 2000a, 2000b]. While observations indicate that smaller marine particles may contain more organic matter, only the larger particles were of optical importance during ACE 1 (Figure 6). Mass closure studies during ACE 1, however, also indicate that up to ≈40% of the dry mass in clean marine aerosol samples may not have been accounted for by inorganic species and may have been organic matter [*Huebert et al.*, 1998; *Quinn and Coffman*, 1998]. Assuming an organic matter density of 1.2 g $cm^{-3}$ [*Turpin and Lim*, 2001] and a dry sea salt density of 2.2 g $cm^{-3}$ [*Lide*, 2000], 10% and 40% of dry mass was estimated to equal 17% and 55% of dry volume, respectively. We then recalculated the total scattering and backscattering coefficients using a refractive index equal to a volume-weighted fraction of the previous inorganic value and an assumed organic value of 1.5 + 0*i* [e.g., *Ross et al.*, 1998]. According to this first-order sensitivity test, model results at the inlet relative humidity were influenced by amounts similar to that induced by experimental uncertainties in other model inputs (see Table 3). The effect on scattering coefficients calculated later at the ambient relative humidity was greater owing to the greater possible impact of organic matter on calculated water uptake (see section 4.2.2).

### 3.3. Evaluation of Point Closure

[38] We evaluated closure for the cases of both spherical particles (with no fit parameters) and nonspherical particles (with fit parameters). To evaluate closure at each point, we compared the difference between the calculated and measured values with the estimated uncertainty in each. First, the error was defined as the calculated value minus the measured value ($\sigma_m - \sigma_o$). Second, the uncertainty in each measurement ($+\Delta\sigma_{o+}/-\Delta\sigma_{o-}$) was estimated as the meas-

**Table 3.** Uncertainty in Measured and Calculated Scattering Coefficients at 550 nm

| Quantity | Ship ($N$ = 887) | | Aircraft ($N$ = 70) | |
|---|---|---|---|---|
| | $\sigma_s$, % | $\sigma_b$, % | $\sigma_s$, % | $\sigma_b$, % |
| Measurement uncertainty[a] | +11.2/−5.2 | +14.2/−10.1 | +15.0/−15.0 | +15.0/−15.0 |
| Calculation uncertainty[b] | | | | |
| Median | +10.5/−3.2 | +10.5/−2.6 | +14.8/−14.3 | +15.8/−15.3 |
| Range | +44.1/−49.7 | +21.5/−34.3 | +24.3/−21.6 | +18.9/−18.8 |
| Inlet temperature ±10% | +0.6/−0.5 | +0.6/−0.7 | +3.3/−0.6 | +3.1/−0.4 |
| Inlet relative humidity ±20% | +42.8/−29.5 | +18.7/−15.3 | +5.4/−4.5 | +3.1/−2.8 |
| Particle sizing ±0−5%[c] | +3.4/−3.1 | +2.8/−2.7 | +21.9/−19.2 | +15.8/−14.5 |
| Particle counting ±1−10%[d] | +3.9/−3.8 | +3.5/−3.5 | +13.9/−16.5 | +13.3/−14.8 |
| Particles not counted[e] | +10.0/−0.0 | +10.0/−0.0 | ... | ... |
| Nephelometer heating[f] | +2.8/−42.2 | +5.0/−31.6 | +0.6/−4.0 | +0.4/−3.0 |
| Composition assumptions | | | | |
| Median[g] | +0.3/−3.6 | +2.2/−3.5 | +9.4/−0.0 | +2.7/−3.1 |
| Range[g] | +41.9/−14.9 | +26.1/−26.2 | +36.6/−3.9 | +48.0/−15.3 |
| Organic, 10%[h] | +2.0/−1.1 | +4.6/−3.5 | +3.4/−1.2 | +5.3/−3.8 |
| Organic, 40%[h] | +6.6/−1.2 | +12.5/−6.4 | +11.1/−3.8 | +17.3/−12.1 |
| Inorganic[i] | +41.9/−14.9 | +26.1/−26.1 | +36.5/−0.7 | +47.9/−13.7 |

[a]On the ship, calculated from *Quinn and Coffman* [1998] without a 1-μm size cut. On the aircraft, estimated to be uniformly at least as high as the highest value on the ship, ≈±15%.

[b]Estimated for each point as the square root of the sum of the squared values found from the sensitivity tests listed below (inlet temperature and relative humidity, particle sizing and counting, and nephelometer heating). Uncertainties associated with chemical composition assumptions not included (see sections 3.2.1 and 3.2.4). All values account for nephelometer nonidealities (to allow comparison with measurements) and particles were assumed spherical.

[c]On the ship, reported DMPS values varied by ±2.5% and uncertainty in reported APS data considered negligible [*Quinn and Coffman*, 1998]. On the aircraft, reported OPC values varied by ±5%.

[d]On the ship, reported DMPS values varied by ±10% and reported APS values varied by ±1% [*Quinn and Coffman*, 1998]. On the aircraft, reported OPC values varied by ±10%.

[e]On the ship, estimated effect of particles larger than 5 μm that were not counted [*Quinn and Coffman*, 1998].

[f]Nephelometer assumed to heat inlet air stream by 5°C and lower relative humidity accordingly.

[g]Median and range for each point estimated as the square root of the sum of the squared values found from the sensitivity tests for 40% organic matter and charge-imbalanced reported chemistry.

[h]Organic matter assumed to account for 10% and 40% of dry particle mass, well-mixed, with a real refractive index of 1.5 (see section 3.2.4).

[i]Model results with charge-imbalanced reported chemistry (see section 3.2.1).

ured value multiplied by the reported instrumental uncertainty range listed in Table 3 (inlet temperature and relative humidity, particle sizing and counting, and nephelometer heating). Third, the uncertainty in each calculated value ($+\Delta\sigma_{m+}/-\Delta\sigma_{m-}$) was estimated as the square root of the sum of the squared positive and negative uncertainties listed in Table 3, evaluated by multiple model runs at each point. Finally, closure was considered to be obtained if the error fell within the range of uncertainty,

$$-(\Delta\sigma_{o-} + \Delta\sigma_{m+}) < (\sigma_m - \sigma_o) < (\Delta\sigma_{o+} + \Delta\sigma_{m-}). \quad (7)$$

Outliers and values near the detection limit were clearly present in some cases (as during day 335 in Figure 3), but we did not attempt to remove them.

[39] The percentage of points at which closure was obtained is reported in Table 4, along with the bias in the calculated scattering coefficients. Generalizing these results on the ship, total scattering closure was usually obtained (>80%), backscattering closure was also usually obtained (>80%) if the particles were assumed nonspherical, and results were similar at all wavelengths. On the aircraft, closure was obtained less frequently (<50%) and the model systematically underestimated measurements by 20−45%. We note several possible reasons for lack of closure and systematic bias on the aircraft. First, a low signal-to-noise ratio appears to be present, especially in the backscattering measurements (e.g., Figure 2f versus Figure 2e), and we have thus likely underestimated the experimental uncertainty in the measured values. Second, small differences in the inlet penetration efficiencies of optically important large particles could have resulted in differences between the aerosols observed by OPC and nephelometer [*Blomquist et al.*, 2001]. And third, the OPC used on the aircraft assumed all submicron particles to be ammonium bisulfate, but this was not accurate in the MBL where optically important submicron particles were sea salt, inducing an error in reported sizes [e.g., *Liu and Daum*, 2000]. All three of these factors can be addressed by modeling corrections, but we did not attempt such corrections due to the small quantity of aircraft data that we examined in this study and the minor effect of aircraft results on the following column closure results.

[40] It is difficult to quantitatively compare our results on the ship with those of *Quinn and Coffman* [1998] owing to the fact that they separately evaluate submicron and supermicron size fractions, in addition to using much longer averaging times. However, qualitatively, we note that they report closure for both total and hemispheric backscattering coefficients for the submicron fraction, which is consistent with our results in the sense that nonsphericity only affected our calculations for the supermicron particles. If their submicron and supermicron results were considered as a sum (neglecting the 1-μm impactor size cut characteristics), it also seems likely that they would have found closure for total scattering but not for backscattering when assuming spherical particles, as found here.

[41] Finally, an important aspect of closure studies is identifying the factors contributing most to uncertainty in

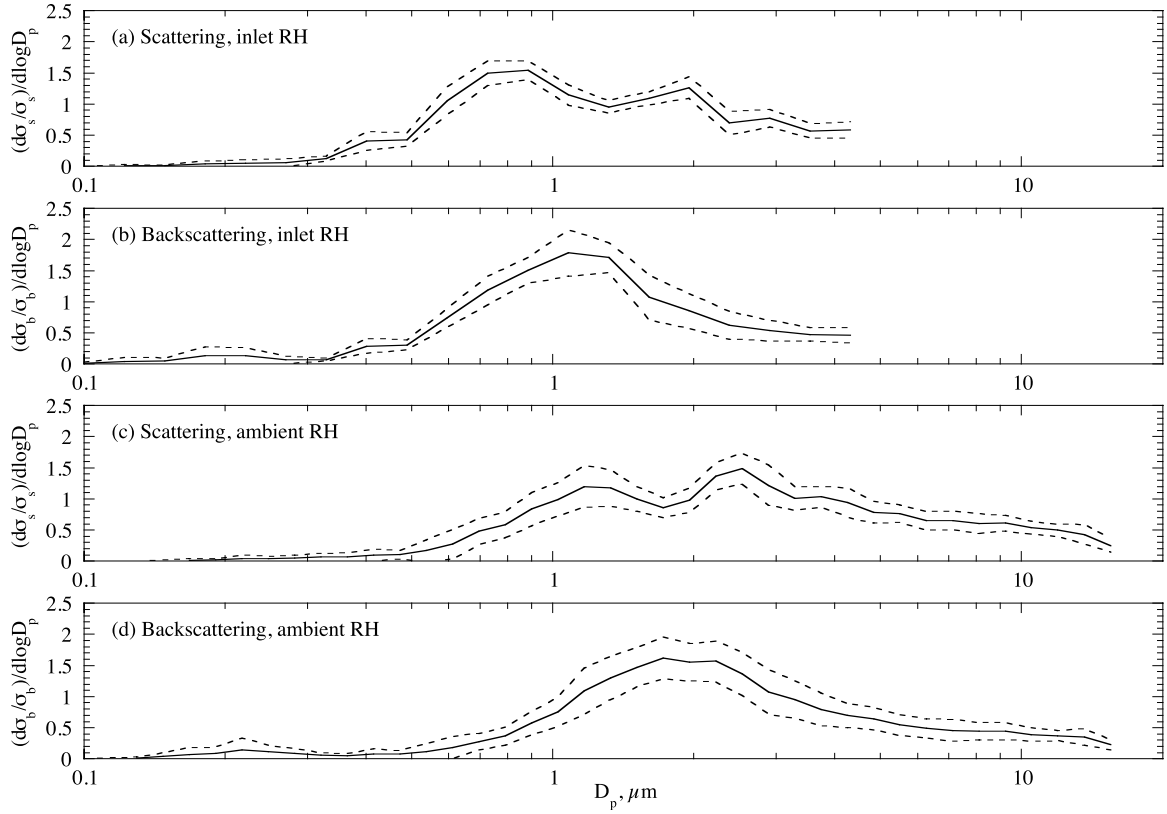


**Figure 6.** The normalized size distribution of the 550-nm total scattering and hemispheric backscattering coefficients on the ship at the inlet relative humidity (a and b) and at the ambient relative humidity (c and d). Given the 887 samples modeled, shown here are the mean contribution of each size (solid lines) plus and minus a standard deviation (dashed lines). When normalized, the scattering size distributions were remarkably uniform throughout the 25-day duration of the ship's cruise.

calculations and deviations from closure. According to the analysis on the ship, the most important factors were (1) uncertainty in the relative humidity owing to inlet measurement uncertainty or possible nephelometer heating, (2) lack of number size distribution data for the largest particles, and (3) assumptions regarding dry particle shape. On the aircraft, where particles were sampled at much drier relative humidity, particle sizing and counting were the most important sources of uncertainty. On both platforms, assumptions regarding inorganic charge-balance and organic content were also of primary importance. However, we believe that we omitted important unknown sources of uncertainty in the aircraft measurements, as discussed above and demonstrated by the low closure frequency.

## 4. Column Closure

[42] We evaluated column closure for the midday period of each of the only two flights during ACE 1 that were near the ship under clear skies. Because of the lack of spatial and

**Table 4.** Point Closure Summary

| | Ship ($N$ = 887) | | | Aircraft ($N$ = 70) | | |
|---|---|---|---|---|---|---|
| Quantity | 450 nm, % | 550 nm, % | 700 nm, % | 450 nm, % | 550 nm, % | 700 nm, % |
| Scattering, spheres | | | | | | |
| Median error[a] | −8.2 | −5.9 | −2.3 | −28.1 | −24.8 | −21.6 |
| Closure obtained[b] | 80 | 85 | 88 | 34 | 44 | 56 |
| Backscattering, spheres | | | | | | |
| Median error | −25.1 | −19.4 | −18.5 | −33.7 | −45.5 | −41.2 |
| Closure obtained | 30 | 49 | 54 | 20 | 11 | 17 |
| Scattering, nonspheres | | | | | | |
| Median error | −3.5 | −3.0 | +0.3 | −25.8 | −23.0 | −19.9 |
| Closure obtained | 86 | 87 | 88 | 43 | 50 | 60 |
| Backscattering, nonspheres | | | | | | |
| Median error | −5.9 | −6.2 | −10.4 | −28.9 | −42.0 | −39.4 |
| Closure obtained | 88 | 88 | 82 | 29 | 14 | 19 |

[a]Median value of the error, defined as the calculated value minus the measured value, expressed as a percentage of the measured value.
[b]Percentage of points for which the error fell within the closure range, as defined by equation (7).

temporal overlap in the observed profiles of aerosols and meteorological conditions during the flights, the aerosol optical depth spectra calculated with a single composite midday profile were compared with the range of measurements made during the midday period of each flight. In the following sections we describe the column model (section 4.1), results and uncertainties (section 4.2), and evaluation of closure (section 4.3).

[43] Whereas the aerosols were modeled under aerosol inlet conditions to evaluate point closure, they were modeled under ambient conditions to evaluate column closure. The difference between aerosol properties under inlet and ambient conditions was greatest in the MBL and is illustrated by the change in normalized scattering coefficient size distributions calculated on the ship (Figure 6).

### 4.1. Column Model Description

[44] In overview, we applied the Mie point model described above to calculate the aerosol extinction profiles from measurements of pressure, temperature, water vapor, and aerosols below ≈5.5 km (the maximum elevation flown by the aircraft). Above 5.5 km, we used SAGE II satellite observations to directly estimate the spectral aerosol extinction profiles. Column aerosol optical depth as a function of wavelength was then calculated as the vertical integral of the full profile of extinction coefficients ($\sigma_e$),

$$\tau(\lambda) = \int_0^\infty \sigma_e(\lambda, z)dz. \quad (8)$$

[45] Below 5.5 km, pressure, temperature, and relative humidity were initialized with the ISS balloon data. We used midday profiles observed with balloons released at 339.085 (41.3°S, 139.6°E) and 342.084 (45.6°S, 144.1°E) during flights 22 and 24, respectively. The 50 m resolution of the ISS balloon profiles was used between the surface and 2 km elevation, permitting fine resolution of the MBL, and 250 m resolution was used between 2 km and 5.5 km. The water vapor concentration was calculated in each layer as the measured relative humidity multiplied by the saturation vapor pressure calculated at the measured layer temperature.

[46] To initialize aerosols below 5.5 km, the height of the MBL was first identified from the aircraft measurements of aerosol number concentration, which showed a marked discontinuity at the top of the MBL. Plotting the number concentrations of particles in several size ranges (0.15, 0.5, 1.0, and 2.0 μm in diameter) during several ascents and descents during each flight resulted in an estimated MBL height of 1400 m during flight 22 and 700 m during flight 24. During flight 22, balloon profiles indicated that the water vapor mixing ratio was virtually uniform from the surface layer until an abrupt decrease to free tropospheric levels at 1400 m, suggesting a relatively well-mixed boundary layer of that height. During flight 24, however, balloon profiles indicated that the water vapor mixing ratio decreased linearly until free tropospheric values were reached at approximately 1500 m, suggesting a poorly mixed lower atmosphere within which aircraft measurements indicated that large aerosols were confined to the lower 700 m, consistent with previous characterizations of the meteorology during the flight [*Russell et al.*, 1998]. We refer to this lower aerosol layer as the MBL with the understanding that this designation is only important to the initialization procedure for the aerosol profiles.

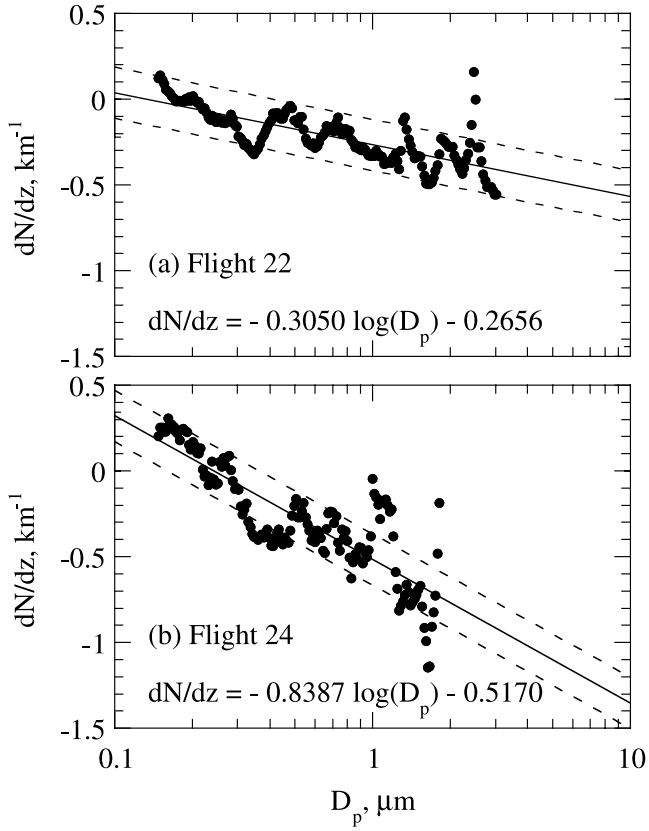


**Figure 7.** The fractional linear change in number concentration with increasing altitude in the MBL as a function of dry particle size, estimated from aircraft measurements during the first descent of each flight (see section 4.1). Equations shown for the log-linear curve fits also derived by least squares regression (solid lines), plus and minus 0.15 estimated uncertainty (dashed lines).

[47] Below the top of the MBL, because optically important particles >3 μm in ambient diameter did not penetrate the aerosol inlet on the aircraft [*Blomquist et al.*, 2001], ship data were used as the basis for initializing aerosols and aircraft data were used only to estimate vertical variability. We used number size distributions measured on the ship at 339.188 and 342.104 during flights 22 and 24, respectively. Observations made on the first aircraft descent during each flight, beginning at 339.162 and 341.874 (see Figure 4), indicated that the particle number concentration often varied approximately linearly with altitude in the MBL. This linear variation was quantified as follows: (1) a linear rate of change of measured particle number concentration with elevation in the MBL was estimated by least squares as a function of particle size, (2) this linear rate was plotted as a function of the logarithm of particle size (Figure 7), and (3) a least-squares line was fit to the plotted data in order to smooth the estimates and extrapolate the observed rates to larger particle sizes. The equation of this line fit (shown for each flight in Figure 7) was then applied to scale the ship data with elevation in the MBL. On both flights, the number

of smallest particles increased with height whereas the number of midsize and large particles decreased with height. Rates of change during each flight were consistent with the meteorological conditions discussed above, indicating a better mixed MBL during flight 22 and a more poorly mixed MBL during flight 24.

[48] Between the top of the MBL and 5.5 km, where particles >3 μm in ambient diameter were negligible, aerosols were initialized directly using the aircraft measurements obtained during the first descent. To predict any increase in aerosol diameters from the drier inlet conditions to the moister ambient conditions in each layer, we applied equation (4) with inlet conditions in place of instrumental conditions and ambient conditions in place of inlet conditions. The point model (see section 3.1) was then used to calculate aerosol extinction profiles.

[49] Above 5.5 km, we used SAGE II satellite observations to directly estimate the aerosol extinction profile. The available profiles closest in time and space to flights 22 and 24 were chosen, measured at 341.466 (53.6°S, 135.1°E) and at 342.403 (51.2°S, 154.8°E), respectively. Thus the nearest available satellite profiles were measured more than 50 hours after the first flight but only several hours after the second flight. Profiles at 385, 453, 525, and 1020 nm were reported down to elevations of 14.5, 9.5, 6.5, and 6.5 km, respectively, on 341.466, and to elevations of 13.5, 9.5, 4.5, and 2.5 km, respectively, on 342.403. To evaluate column closure, we made extrapolations to 453 nm and 5.5 km by first extending the available spectrum at each elevation assuming the spectral shape measured at 20.5 km (where it best matched in situ calculations, as discussed below in section 4.2.1) and then by assuming 5.5 km spectra to be identical to 6.5 km spectra when measurements were not available at any wavelength. We tried other methods of extrapolation and found differences to be small since the extrapolations were not extensive. Satellite data were linearly interpolated from the reported wavelengths (453, 525, and 1020 nm) to the wavelengths at which aerosol optical depth was measured (500, 778, and 862 nm).

[50] After estimating the aerosol extinction profiles during flights 22 and 24, we compared the aerosol optical depths calculated from equation (8) with the multiple 3-wavelength spectra that were reported at midday during each flight. During flight 22, 10 measurements of the optical depth spectrum were made between 339.069 and 339.250. Three of the measured spectra contained values deviating by more than a factor of two from all other measurements at that wavelength and we excluded those spectra. During flight 24, only two spectra were measured, at 342.047 and 342.152, and the two values at each wavelength varied from one another by less than a factor of two.

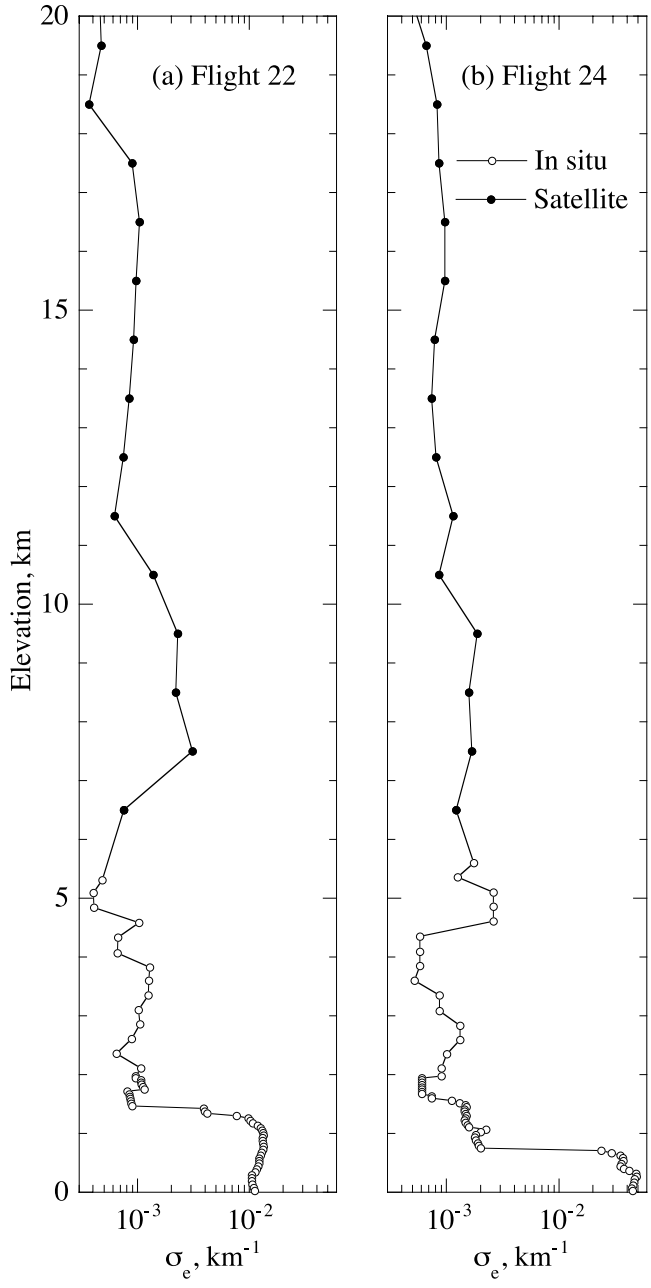


**Figure 8.** Profiles of aerosol extinction coefficients calculated from in situ aircraft measurements in the MBL and lower FT (500 nm) and measured in the upper FT and stratosphere by the SAGE II satellite (525 nm).

### 4.2. Column Model Results

[51] In this section we describe the only adjustment we made to measurements during evaluation of column closure. Namely, after noting deviations between the extinction spectra reported from the SAGE II satellite in the FT and the extinction spectra that we calculated from the in situ ACE 1 aircraft data at similar elevations, we scaled the satellite data to reflect the spectral shape that we calculated (section 4.2.1). The aerosol extinction profiles that we used for both column closure cases are shown in Figure 8 at 525 nm, where spectral scaling had no influence. At the end of this section we summarize the sensitivity of column calculations to experimental uncertainties and model assumptions (section 4.2.2).

#### 4.2.1. SAGE II Spectral Scaling

[52] We first used the dry aerosol size distributions measured by ship and aircraft to initialize the Mie model to the maximum altitude of ≈5.5 km reached on each flight and calculate the extinction coefficients at the measured ambient temperature and relative humidity (Figure 8). When these profiles were integrated to the top of the MBL, ≈1400 km and ≈700 km on the two respective flights, a spectrally

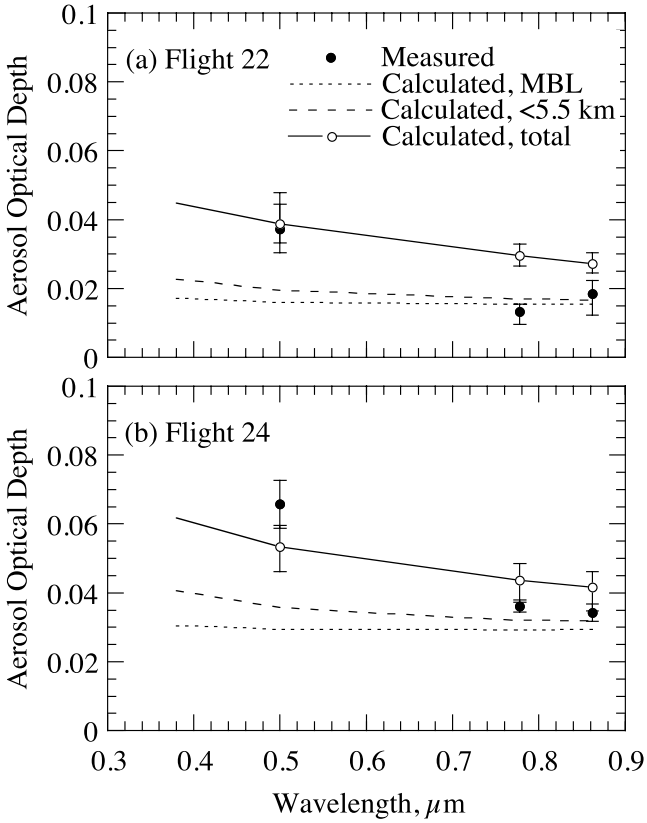


**Figure 9.** Calculated and measured aerosol optical depth as a function of wavelength. Calculated values integrated from the surface to the top of the MBL during each flight (dotted lines), integrated to the maximum aircraft elevation (dashed lines), and further integrated to the top of the atmosphere using the SAGE II measurements (solid lines with open circles). Measurements made on the ship (filled circles) and total calculated values (open circles) are shown with error bars derived as described in section 4.3.

neutral optical depth of 0.01–0.03 was obtained for that layer (dotted lines in Figure 9), consistent with expectations for a remote marine aerosol population dominated by large particles [e.g., *Vitale et al.*, 2000]. When integration was continued upward to the maximum height at which aerosols were measured in situ in the FT (dashed lines in Figure 9), the calculated aerosol optical depth remained substantially lower than that measured at 500 nm (filled circles in Figure 9), as well as more spectrally neutral. When the aerosol extinction profiles measured by the SAGE II satellite (see section 2.3) were then added, the calculated total aerosol optical depth matched measurements fairly well at 500 nm, but consistently overestimated the measurements at longer wavelengths (open circles in Figure 9).

[53] For two reasons we hypothesized that SAGE II measurements reported at the longer wavelengths may have exceeded the true values. First, the SAGE II extinction spectra changed substantially with decreasing elevation in the FT as they approached the lowest levels to which retrievals extended, no longer peaking at the shortest wavelengths and becoming more neutral. And second, the SAGE II extinction spectra measured in the lower FT deviated from the extinction spectra that we calculated in the lower FT using the in situ aircraft measurements. Both of these effects are illustrated in Figure 10 for flight 24, during which SAGE II measurements were temporally and geographically nearest to in situ aircraft measurements.

[54] Following *Stevermer et al.* [2000], who found that SAGE II data were most reliable at 525 nm, we then scaled the satellite data reported at other wavelengths to the extinction spectrum that we calculated in the lower FT. In situ model results were averaged over elevation above the MBL to reduce reliance on individual aircraft measurements (shown by the solid line in Figure 10 for flight 24). Total aerosol optical depth derived in this manner more closely matched measurements at longer wavelengths (Figure 11). In addition to correcting for possible SAGE II overestimation of actual optical depth at 1020 nm, scaling allowed better estimation of the curvature in spectral optical depth between 525 and 1020 nm than was permitted by linear interpolation.

[55] It was difficult to ascertain whether the reported SAGE II extinction spectra were actually high at longer wavelengths, as hypothesized, since most studies have focused on stratospheric optical depths [e.g., *Stevermer et al.*, 2000]. The tropopause elevation reported with each profile shown in Figure 8 was 9 km, for instance, which would exclude the spectral contribution of the aerosols occupying elevations of 5.5–9 km. Additionally, while stratospheric aerosols during late 1995 did not remain significantly volcanically influenced [e.g., *Dutton and Bodhaine*, 2001], influences on the extinction spectrum may outlast influences on other aerosol properties [*Russell et al.*, 1996].

#### 4.2.2. Column Sensitivity Tests

[56] To evaluate closure, it was again necessary to determine the effect of input uncertainties on calculated aerosol optical depth. Table 5 summarizes the total uncertainty derived from the estimated uncertainty in aerosol measurements and other model inputs, including measurement of the particle size distributions, inlet and ambient temperature

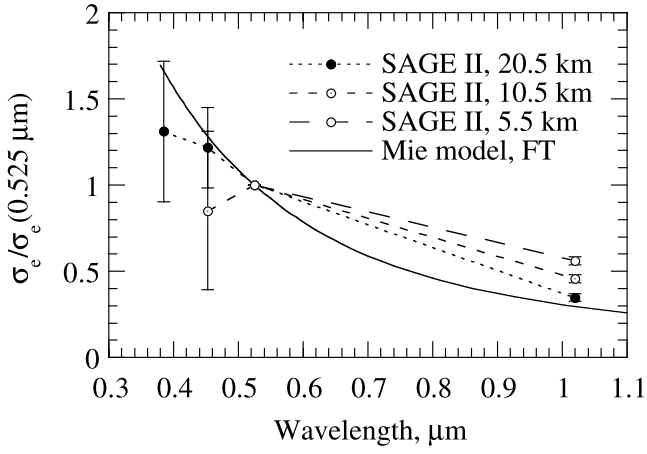


**Figure 10.** Extinction spectra measured by the SAGE II satellite and calculated in the FT using in situ aircraft measurements during flight 24 (see section 4.2.1). Error bars derived from reported SAGE II experimental uncertainty. SAGE II spectra at 10.5 and 5.5 km not reported at wavelengths shorter than 453 and 525 nm, respectively.

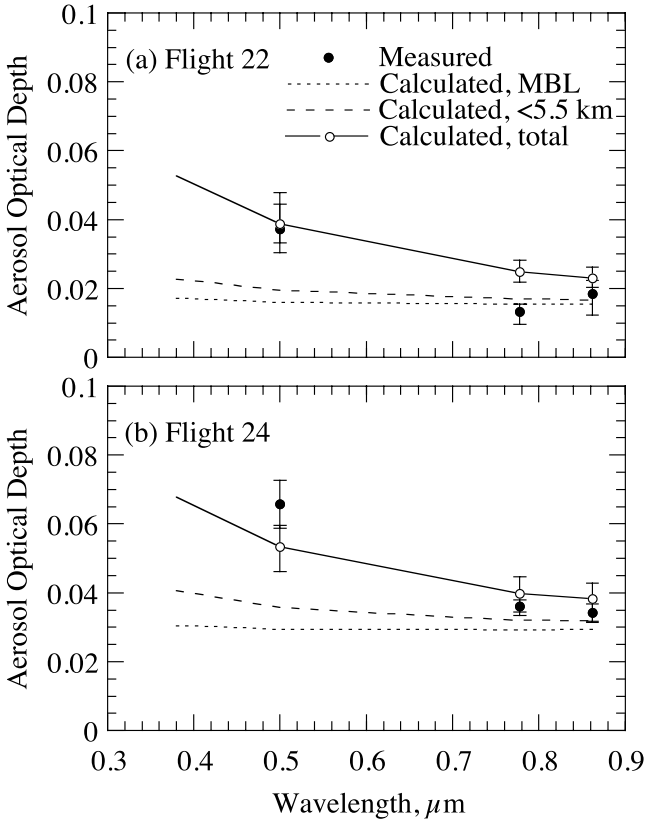


**Figure 11.** Same as Figure 9, except that satellite measurements were spectrally scaled as described in section 4.2.1.

and relative humidity, and MBL parameters. As for point closure, we assumed chemical composition to be "true" and we also made a first-order estimate of the possible effect of organics on the model results in the MBL. Namely, we again assumed that 10% and 40% of dry aerosol mass was organic matter (see section 3.2.4) and then estimated the effect of those organics on both hygroscopicity and refractive index. To make the most conservative estimate of the effect of hygroscopicity, the organics were assumed to be entirely nonhygroscopic. In the hydrated particles under ambient conditions, they were thus assumed to occupy a spherical shell with a volume equal to their original dry volume and the assumed refractive index of organic matter. When estimated in this manner, organics lowered the calculated aerosol optical depth below 5.5 km by 5–30%, primarily in response to the reduced hygroscopicity of the aerosols.

### 4.3. Evaluation of Column Closure

[57] We evaluated closure for both reported and scaled SAGE II measurements. The uncertainty in measured aerosol optical depth was estimated to be the difference between the mean and the range that was measured at each wavelength during a given flight (see section 4.1), conservatively neglecting the experimental uncertainty in the individual measurements. The uncertainty in calculated aerosol optical depth was estimated as a several-step process. First, the uncertainty in Mie model results below 5.5 km was estimated as the square root of the sum of the squared uncertainties listed in Table 5 (ambient temperature and relative humidity, inlet temperature and relative humidity, particle sizing and counting, and MBL profile and height).

**Table 5.** Uncertainty in Measured and Calculated Optical Depth

| | Column ($N$ = 2) | | |
|---|---|---|---|
| Quantity | 500 nm, % | 778 nm, % | 862 nm, % |
| Measurement uncertainty[a] | +27.5/−19.4 | +18.6/−26.4 | +26.7/−28.1 |
| Calculation uncertainty[b] | +14.9/−14.0 | +11.5/−14.8 | +11.5/−16.5 |
| Satellite uncertainty[c] | +24.8/−24.8 | +15.1/−15.1 | +13.0/−13.0 |
| Mie model uncertainty | | | |
| Total range[d] | +16.7/−17.1 | +16.7/−19.3 | +16.9/−21.3 |
| Ambient temperature ±0.4°C | +0.4/−0.3 | +0.3/−0.2 | +0.3/−0.2 |
| Ambient relative humidity ±2% | +5.4/−4.5 | +5.0/−4.8 | +5.9/−4.7 |
| Inlet temperature ±10% | +0.7/−0.8 | +0.7/−0.8 | +0.8/−0.8 |
| Inlet relative humidity ±20% | +0.2/−13.2 | +0.3/−16.0 | +0.2/−18.3 |
| Particle sizing ±0–5% | +4.9/−4.1 | +2.6/−2.1 | +2.2/−1.7 |
| Particle counting ±1–10% | +4.8/−4.7 | +3.0/−3.0 | +2.6/−2.6 |
| Particles not counted | +10.0/−0.0 | +10.0/−0.0 | +10.0/−0.0 |
| MBL profile ±15%[e] | +10.8/−10.8 | +12.1/−12.1 | +12.4/−12.4 |
| MBL height ±15%[f] | +4.0/−6.2 | +4.6/−7.0 | +4.6/−7.1 |
| Composition assumptions | | | |
| MBL organic, 10%[g] | +0.0/−7.6 | +0.0/−8.4 | +0.0/−8.5 |
| MBL organic, 40%[g] | +0.0/−27.5 | +0.0/−28.8 | +0.0/−29.4 |

[a]Range of the uncertainties estimated as the difference between the mean value and the minimum and maximum values measured at each wavelength on each flight.

[b]Range of the uncertainties estimated as the square root of the sum of the squared uncertainties found for satellite profiles (>5.5 km) and model profiles (<5.5 km).

[c]Range of the integrated uncertainties reported with the SAGE II data at each wavelength.

[d]Range of uncertainties estimated as the square root of the sum of the squared uncertainties found from the sensitivity tests listed below (inlet and ambient temperature and relative humidity, particle sizing and counting, and MBL profile and height). Input uncertainties same as in Table 3 unless otherwise indicated.

[e]Rate of change in dry particle number concentration with height in the MBL varied by ±15% (see Figure 7).

[f]MBL height estimated from the aircraft data (see section 3.1) varied by ±15%.

[g]Organic matter assumed to account for 10% and 40% of dry particle mass in the MBL, nonhygroscopic, occupying an outer shell with a real refractive index of 1.5 (see section 4.2.2).

Second, the reported uncertainties in the satellite measurements were integrated to estimate uncertainty as a function of wavelength in the column above 5.5 km. Third, the uncertainty in the total calculated optical depth was estimated as the square root of the sum of the squared uncertainties in both Mie model results (<5.5 km) and satellite profiles (>5.5 km).

[58] Column closure was obtained on both flights at 500 nm (Figure 9), but was not obtained at any longer wavelengths during flight 22 unless SAGE II measurements were scaled to in situ model results (Figure 11). The factors contributing most to uncertainty in calculated aerosol optical depth and deviations from column closure were (1) experimental uncertainty in the satellite extinction coefficient profiles, (2) experimental uncertainty in inlet relative humidity, (3) uncertainty in estimated dry particle number concentration profiles in the MBL, and (4) lack of number size distribution data on the ship for the largest particles. Depending upon day and wavelength, estimated to be of almost equal importance were the uncertainty in ambient relative humidity profiles, particle sizing and counting, and MBL height (Table 5). Assuming 10% organic content affected calculated aerosol optical depth by the same order of magnitude as other experimental uncertainties, but assuming 40% organic content affected calculations by more than any other source of uncertainty considered here.

## 5. Conclusions

[59] The primary conclusions of the studies reported above may be summarized as follows:

1. On the ship, point closure was usually obtained (>80%) for the total aerosol scattering coefficient with low overall bias (<10%) at all wavelengths. Since experimental uncertainties often account for a single standard deviation of repeated measurements, containing ≈68% of the values of a normally distributed variable, this might be considered full closure.

2. On the ship, point closure was less successfully obtained (<50%) for the hemispheric backscattering coefficient with high negative bias (15–25%) at all wavelengths when particles were assumed spherical, but when a model for particle nonsphericity was fit, closure was usually obtained (>80%) for backscattering with low overall bias (<10%) at all wavelengths. Additional laboratory investigations would be required to corroborate that nonsphericity of the dried sea salt aerosols was in fact responsible for enhanced backscattering. Since the atmospheric radiation budget is expected to be sensitive to aerosol backscattering [e.g., *Marshall et al.*, 1995], considering nonsphericity may be important to correct interpretation of field measurements and correct application of measured quantities to larger-scale climate models. Also, while solids are not likely present at significant quantities under the moist ambient conditions in the MBL, observations indicate that crystallized sea salt may occur under ambient coastal conditions [*Murayama et al.*, 1999].

3. On the aircraft, point closure was usually not obtained (<50%) with a high negative bias (20–45%) for both total scattering and backscattering coefficients, regardless of assumed particle shape. Future study with additional available ACE 1 aircraft data could investigate whether this may have been due to differences in the aerosol inlet penetration efficiencies to each instrument or unidentified uncertainties in the measured number size distributions or scattering coefficients.

**Table 6.** Calculated Backscattered Fraction on the Ship at 550 nm

| Leg 2 Average | 22% Relative Humidity, Spheres | 22% Relative Humidity, Nonspheres | 82% Relative Humidity, Spheres |
|---|---|---|---|
| Inlet value | 0.108 | 0.119 | 0.072 |
| Nephelometer value | 0.132 | 0.148 | 0.097 |
| Correction method 1[a] | 0.101 | 0.112 | 0.074 |
| Correction method 2[b] | 0.094 | 0.106 | 0.070 |

[a]Using linear correction factors from Table 4a of *Anderson and Ogren* [1998] for both total scattering and backscattering coefficients.

[b]Using angstrom correction factors from Table 4b of *Anderson and Ogren* [1998] for total scattering coefficients and linear correction factors from Table 4a for backscattering coefficients.

4. Documented nephelometer nonidealities resulted in large deviations between the total scattering coefficients calculated under inlet and nephelometer conditions. While nonidealities generally have less effect on measured hemispheric backscattering, they may have a more pronounced effect on the reported values of the backscattered fraction, $b$, to which climate models are sensitive. We numerically tested the state-of-the-art data correction methods for the nephelometer on the ship at 550 nm, using both linear and angstrom correction coefficients for total scattering [*Anderson and Ogren*, 1998]. The calculated $b$ values under nephelometer conditions were 20–35% lower than under inlet conditions (Table 6), depending upon relative humidity and assumed dry particle shape. Both correction methods brought the calculated nephelometer $b$ values closer to the calculated inlet values, but deviations still exceeded 10% under the coarse-mode dominated ACE 1 conditions if angstrom correction coefficients were used at the dry relative humidity.

5. Column closure was obtained at 500 nm on both days studied, as well as at longer wavelengths on the second day. Calculated spectral optical depths were usually within 25% of measurements and agreement at longer wavelengths was improved when satellite measurements were spectrally scaled using in situ model results.

6. On both days that column closure was evaluated, free tropospheric and stratospheric aerosols appeared to contribute significantly to total aerosol optical depth at 500 nm. These aerosols above the MBL also determined the curvature in the calculated aerosol optical depth spectra, which were otherwise neutral due to the predominance of large particles in the MBL.

7. An important source of uncertainty in both point and column closure studies was the lack of number size distribution data for the largest particles on both ship and aircraft (Figures 6a and 6b). *O'Dowd et al.* [1997] note that the full number size distribution is difficult to measure in marine environments due to the broad size range but essential to establish in future studies.

[60] **Acknowledgments.** This work was supported by National Science Foundation Agreements ATM-9504481 and ATM-9614118, National Aeronautics and Space Administration Agreement NIP-0000-0003, and a Stanford University Lieberman Dissertation Fellowship. We are grateful for data provided by Patricia Quinn and Timothy Bates (aerosol chemical composition, number size distributions, light scattering coefficients, optical

depth, and meteorological variables on the ship), Tony Clarke (aerosol number size distributions and light scattering coefficients on the aircraft), Barry Huebert (aerosol chemical composition on the aircraft), Alan Schanot (meteorological variables on the aircraft), Tad Anderson (nephelometer performance data), and the National Aeronautics and Space Administration Langley Research Center Radiation and Aerosols Branch (SAGE II aerosol extinction coefficient profiles).

## References

Anderson, T. L., and J. A. Ogren, Determining aerosol radiative properties using the TSI 3563 integrating nephelometer, *Aerosol Sci. Technol.*, *29*, 57–69, 1998.

Anderson, T. L., et al., Performance characteristics of a high-sensitivity, three-wavelength total scatter/backscatter nephelometer, *Atmos. Oceanic Technol.*, *13*, 967–986, 1996.

Ayers, G. P., R. W. Gillett, J. M. Cainey, and A. L. Dick, Chloride and bromide loss from sea-salt particles in Southern Ocean air, *J. Atmos. Chem.*, *33*, 299–319, 1999.

Bates, T. S., B. J. Huebert, J. L. Gras, F. B. Griffiths, and P. A. Durkee, International Global Atmospheric Chemistry (IGAC) Project's First Aerosol Characterization Experiment (ACE 1): Overview, *J. Geophys. Res.*, *103*, 16,297–16,318, 1998a.

Bates, T. S., V. N. Kapustin, P. K. Quinn, D. S. Covert, D. J. Coffman, C. Mari, P. A. Durkee, W. J. DeBruyn, and E. S. Saltzman, Processes controlling the distribution of aerosol particles in the lower marine boundary layer during the First Aerosol Characterization Experiment (ACE 1), *J. Geophys. Res.*, *103*, 16,369–16,383, 1998b.

Baumgardner, D., and A. Clarke, Changes in aerosol properties with relative humidity in the remote Southern Hemisphere marine boundary layer, *J. Geophys. Res.*, *103*, 16,525–16,534, 1998.

Berg, O. H., E. Swietlicki, and R. Krejci, Hygroscopic growth of aerosol particles in the marine boundary layer over the Pacific and Southern Oceans during the First Aerosol Characterization Experiment (ACE 1), *J. Geophys. Res.*, *103*, 16,535–16,545, 1998.

Blomquist, B. W., B. J. Huebert, S. G. Howell, M. R. Litchy, C. H. Twohy, A. Schanot, D. Baumgardner, B. Lafleur, R. Seebaugh, and M. L. Laucks, An evaluation of the Community Aerosol Inlet for the NCAR C-130 Research Aircraft, *J. Atmos. Oceanic Technol.*, *18*, 1387–1397, 2001.

Bohren, C. F., and D. R. Huffman, *Absorption and Scattering of Light by Small Particles*, John Wiley, New York, 1983.

Bohren, C. F., and S. B. Singham, Backscattering by nonspherical particles: A review of methods and suggested new approaches, *J. Geophys. Res.*, *96*, 5269–5277, 1991.

Cheng, Y. S., B. T. Cheng, and H. C. Yeh, Behaviour of isometric nonspherical aerosol particles in the aerodynamic particle sizer, *J. Aerosol Sci.*, *21*, 701–710, 1990.

Clarke, A. D., J. N. Porter, F. P. J. Valero, and P. Pilewski, Vertical profiles, aerosol microphysics, and optical closure during the Atlantic Stratocumulus Transition Experiment: Measured and modeled column optical properties, *J. Geophys. Res.*, *101*, 4443–4453, 1996.

Clarke, A. D., J. L. Varner, F. Eisele, R. L. Mauldin, D. Tanner, and M. Litchy, Particle production in the remote marine atmosphere: Cloud outflow and subsidence during ACE 1, *J. Geophys. Res.*, *103*, 16,397–16,409, 1998.

Collins, D. R., H. H. Jonsson, H. Liao, R. C. Flagan, J. H. Seinfeld, K. J. Noone, and S. V. Hering, Airborne analysis of the Los Angeles aerosol, *Atmos. Environ.*, *34*, 4155–4173, 2000a.

Collins, D. R., et al., In situ aerosol-size distributions and clear-column radiative closure during ACE-2, *Tellus, Ser. B*, *52*, 498–525, 2000b.

Dutton, E. G., and B. A. Bodhaine, Solar irradiance anomalies caused by clear-sky transmission variations above Mauna Loa: 1958–99, *J. Clim*, *14*, 3255–3262, 2001.

Ebert, M., S. Weinbruch, P. Hoffmann, and H. M. Ortner, Chemical characterization of North Sea aerosol particles, *J. Aerosol Sci.*, *31*, 613–632, 2000.

Fridlind, A. M., and M. Z. Jacobson, A study of gas-aerosol equilibrium and aerosol pH in the remote marine boundary layer during the First Aerosol Characterization Experiment (ACE 1), *J. Geophys. Res.*, *105*, 17,325–17,340, 2000.

Hartley, W. S., P. V. Hobbs, J. L. Ross, P. B. Russell, and J. M. Livingston, Properties of aerosols aloft relevant to direct radiative forcing off the mid-Atlantic coast of the United States, *J. Geophys. Res.*, *105*, 9859–9885, 2000.

Heintzenberg, J., and R. J. Charlson, Design and applications of the integrating nephelometer: A review, *J. Atmos. Oceanic Technol.*, *13*, 987–1000, 1996.

Hinds, W. C., *Aerosol Technology*, John Wiley, New York, 1982.

Huebert, B. J., S. G. Howell, L. Zhuang, J. A. Heath, M. R. Litchy, D. J. Wylie, J. L. Kreidler-Moss, S. Cöppicus, and J. E. Pfeiffer, Filter and impactor measurements of anions and cations during the First Aerosol Characterization Experiment (ACE 1), *J. Geophys. Res.*, *103*, 16,493–16,509, 1998.

Intergovernmental Panel on Climate Change, *Climate Change 2001: The Scientific Basis*, Cambridge Univ. Press, New York, 2001.

Jacobson, M. Z., *Fundamentals of Atmospheric Modeling*, Cambridge Univ. Press, New York, 1999a.

Jacobson, M. Z., Studying the effects of calcium and magnesium on size-distributed nitrate and ammonium with EQUISOLV II, *Atmos. Environ.*, *33*, 3635–3649, 1999b.

Kelly, W. P., and P. H. McMurry, Measurement of particle density by inertial classification of differential mobility analyzer-generated monodisperse aerosols, *Aerosol Sci. Technol.*, *17*, 199–212, 1992.

Lide, D. R., (Ed.), *Chemical Rubber Company Handbook of Chemistry and Physics*, 81st ed., CRC Press, Boca Raton, Fla., 2000.

Liu, Y., and P. H. Daum, The effect of refractive index on size distributions and light scattering coefficients derived from optical particle counters, *J. Aerosol Sci.*, *31*, 945–957, 2000.

Marshall, I. A., J. P. Mitchell, and W. D. Griffiths, The behaviour of regular-shaped non-spherical particles in a TSI aerodynamic particle sizer, *J. Aerosol Sci.*, *22*, 73–89, 1991.

Marshall, S. F., D. S. Covert, and R. J. Charlson, Relationship between asymmetry parameter and hemispheric backscatter ratio: Implications for climate forcing by aerosols, *Appl. Opt.*, *34*, 6306–6311, 1995.

McInnes, L. M., D. S. Covert, P. K. Quinn, and M. S. Germani, Measurements of chloride depletion and sulfur enrichment in individual sea-salt particles collected from the remote marine boundary layer, *J. Geophys. Res.*, *99*, 8257–8268, 1994.

Middlebrook, A. M., D. M. Murphy, and D. S. Thomson, Observations of organic material in individual marine particles at Cape Grim during the First Aerosol Characterization Experiment (ACE 1), *J. Geophys. Res.*, *103*, 16,475–16,483, 1998.

Murayama, T., H. Okamoto, N. Kaneyasu, H. Kamataki, and K. Miura, Application of lidar depolarization measurement in the atmospheric boundary layer: Effects of dust and sea-salt particles, *J. Geophys. Res.*, *104*, 31,781–31,792, 1999.

Murphy, D. M., J. R. Anderson, P. K. Quinn, L. M. McInnes, F. J. Brechtel, S. M. Kreidenweis, A. M. Middlebrook, M. Pósfai, D. S. Thomson, and P. R. Buseck, Influence of sea-salt on aerosol radiative properties in the Southern Ocean marine boundary layer, *Nature*, *392*, 62–65, 1998.

Neusüß, C., M. Pelzing, A. Plewka, and H. Herrmann, A new analytical approach for size-resolved speciation of organic compounds in atmospheric aerosol particles: Methods and first results, *J. Geophys. Res.*, *105*, 4513–4527, 2000a.

Neusüß, C., D. Weise, W. Birmili, H. Wex, A. Wiedensohler, and D. S. Covert, Size-segregated chemical, gravimetric and number distribution-derived mass closure of the aerosol in Sagres, Portugal during ACE-2, *Tellus, Ser. B*, *52*, 169–184, 2000b.

O'Dowd, C. D., M. H. Smith, I. E. Consterdine, and J. A. Lowe, Marine aerosol, sea-salt, and the marine sulphur cycle: A short review, *Atmos. Environ.*, *31*, 73–80, 1997.

Oppo, C., S. Bellandi, N. Degli Innocenti, A. M. Stortini, G. Loglio, E. Schiavuta, and R. Cini, Surfactant components of marine organic matter as agents for biogeochemical fractionation and pollutant transport via marine aerosols, *Mar. Chem.*, *63*, 235–253, 1999.

Perry, R. J., A. J. Hunt, and D. R. Huffman, Experimental determinations of Mueller scattering matrices for nonspherical particles, *Appl. Opt.*, *17*, 2700–2710, 1978.

Pilinis, C., and X. Li, Particle shape and internal inhomogeneity effects on the optical properties of tropospheric aerosols of relevance to climate forcing, *J. Geophys. Res.*, *103*, 3789–3800, 1998.

Pollack, J. B., and J. N. Cuzzi, Scattering by nonspherical particles of size comparable to a wavelength: A new semi-empirical theory and its application to tropospheric aerosols, *J. Atmos. Sci.*, *37*, 868–881, 1980.

Pósfai, M., J. R. Anderson, P. R. Buseck, T. W. Shattuck, and N. W. Tindale, Constituents of a remote Pacific marine aerosol study: A TEM study, *Atmos. Environ.*, *28*, 1747–1756, 1994.

Quinby-Hunt, M. S., L. L. Erskine, and A. J. Hunt, Polarized light scattering by aerosols in the marine atmospheric boundary layer, *Appl. Opt.*, *36*, 5168–5184, 1997.

Quinn, P. K., and D. J. Coffman, Local closure during the First Aerosol Characterization Experiment (ACE 1): Aerosol mass concentration and scattering and backscattering coefficients, *J. Geophys. Res.*, *103*, 16,575–16,596, 1998.

Quinn, P. K., S. F. Marshall, T. S. Bates, D. S. Covert, and V. N. Kapustin, Comparison of measured and calculated aerosol properties relevant to the direct radiative forcing of tropospheric sulfate aerosol on climate, *J. Geophys. Res.*, *100*, 8977–8991, 1995.

Quinn, P. K., T. L. Anderson, T. S. Bates, R. Dlugi, J. Heintzenberg, W. von Hoyningen-Huene, M. Kulmala, P. B. Russell, and E. Swietlicki, Closure in tropospheric aerosol-climate research: A review and future needs for addressing aerosol direct shortwave radiative forcing, *Beitr. Phys. Atmos.*, *69*, 547–577, 1996a.

Quinn, P. K., V. N. Kapustin, T. S. Bates, and D. S. Covert, Chemical and optical properties of marine boundary layer aerosol particles of the mid-Pacific in relation to sources and meteorological transport, *J. Geophys. Res.*, *101*, 6931–6951, 1996b.

Quinn, P. K., D. J. Coffman, V. N. Kapustin, T. S. Bates, and D. S. Covert, Aerosol optical properties in the marine boundary layer during the First Aerosol Characterization Experiment (ACE 1) and the underlying chemical and physical aerosol properties, *J. Geophys. Res.*, *103*, 16,547–16,563, 1998.

Quinn, P. K., D. J. Coffman, T. S. Bates, T. L. Miller, J. E. Johnson, K. Voss, E. J. Welton, and C. Neusüß, Dominant aerosol chemical components and their contribution to extinction during the Aerosols99 cruise across the Atlantic, *J. Geophys. Res.*, *106*, 20,783–20,809, 2001.

Ross, J. L., P. V. Hobbs, and B. Holben, Radiative characteristics of regional hazes dominated by smoke from biomass burning in Brazil: Closure tests and direct radiative forcing, *J. Geophys. Res.*, *103*, 31,925–31,941, 1998.

Russell, P. B., and J. Heintzenberg, An overview of the ACE-2 clear sky column closure experiment (CLEARCOLUMN), *Tellus, Ser. B*, *52*, 463–483, 2000.

Russell, P. B., et al., Global to microscale evolution of the Pinatubo volcanic aerosol derived from diverse measurements and analyses, *J. Geophys. Res.*, *101*, 18,745–18,763, 1996.

Russell, L. M., D. H. Lenschow, K. K. Laursen, P. B. Krummel, S. T. Siems, A. R. Bandy, D. C. Thornton, and T. S. Bates, Bidirectional mixing in an ACE 1 marine boundary layer overlain by a second turbulent layer, *J. Geophys. Res.*, *103*, 16,411–16,432, 1998.

Stevermer, A. J., I. V. Petropavlovskikh, J. M. Rosen, and J. J. DeLuisi, Development of a global stratospheric aerosol climatology: Optical properties and applications for UV, *J. Geophys. Res.*, *105*, 22,763–22,776, 2000.

Stumm, W., and J. J. Morgan, *Aquatic Chemistry*, John Wiley, New York, 1996.

Tang, I. N., H. R. Munkelwitz, and J. G. Davis, Aerosol growth studies, II, Preparation and growth measurements of monodisperse salt aerosols, *J. Aerosol Sci.*, *8*, 149–159, 1977.

Tang, I. N., A. C. Tridico, and K. H. Fung, Thermodynamic and optical properties of sea salt aerosols, *J. Geophys. Res.*, *102*, 23,269–23,275, 1997.

Toon, O. B., and T. P. Ackerman, Algorithms for the calculation of scattering by stratified spheres, *Appl. Opt.*, *20*, 3657–3660, 1981.

Turpin, B. J., and H. J. Lim, Species contributions to PM2.5 mass concentrations: Revisiting common assumptions for estimating organic mass, *Aerosol Sci. Technol.*, *35*, 602–610, 2001.

Vitale, V., C. Tomasi, W. von Hoyningen-Huene, U. Bonafe, S. Marani, A. Lupi, A. Cacciari, and P. Ruggeri, Spectral measurements of aerosol particle extinction in the 0.4–3.7 wavelength range, performed at Sagres with the IR-RAD sun-radiometer, *Tellus, Ser. B*, *52*, 716–733, 2000.

von Hoyningen-Huene, W., and P. Posse, Nonsphericity of aerosol particles and their contribution to radiative forcing, *J. Quant. Spectrosc. Radiat. Transfer*, *57*, 651–668, 1997.

Weis, D. D., and G. E. Ewing, Water content and morphology of sodium chloride aerosol particles, *J. Geophys. Res.*, *104*, 21,275–21,285, 1999.

Whittlestone, S., J. L. Gras, and S. T. Siems, Surface air mass origins during the First Aerosol Characterizations Experiment (ACE 1), *J. Geophys. Res.*, *103*, 16,341–16,350, 1998.

A. M. Fridlind, Earth Science Division, Mail Stop 245-4, NASA Ames Research Center, Moffett Field, CA 94035, USA. (fridlind@ice.arc.nasa.gov)

M. Z. Jacobson, Department of Civil and Environmental Engineering, Stanford University, Stanford, CA 94305-4020, USA. (jacobson@ce.stanford.edu)